

Relative rates of reaction of
pyrite and marcasite
with ferric iron at low pH

by

Cynthia Leigh Wiersma

Thesis submitted to the Faculty of
Virginia Polytechnic Institute and State University
in partial fulfillment of the requirements of the degree of

MASTER OF SCIENCE

in

Geology

APPROVED:

J. D. Rimstidt, Chairman

G. V. Gibbs

J. R. Craig

December, 1982
Blacksburg, Virginia

ACKNOWLEDGEMENTS

The author gratefully acknowledges the following individuals for their contributions to this study: J. D. Rimstidt for his guidance and support throughout the duration of the project; J. F. Light and D. N. Bodell for their expert technical assistance; G. V. Gibbs and J. R. Craig for their constructive comments on the original manuscript; O. Whaley and S. Chiang, who drafted the final figures and H. L. Barnes of the Pennsylvania State University Department of Geochemistry and Mineralogy, who kindly provided access to the Quantachrome Quantasorb. Mike McKibben provided valuable technical assistance with the BET-method of surface area measurement and engaged in several helpful discussions on the topic of this study.

This work was supported by Virginia MMRRI Grant No. G1106007.

TABLE OF CONTENTS

ACKNOWLEDGEMENTS	ii
LIST OF FIGURES	iv
LIST OF TABLES	v
CHAPTER 1; INTRODUCTION	1
CHAPTER 2; PREVIOUS STUDIES	6
CHAPTER 3; EXPERIMENTAL	11
CHAPTER 4; CALCULATION OF THE RATE CONSTANTS	19
CHAPTER 5; DISCUSSION OF RESULTS	26
CHAPTER 6; CONCLUSIONS	36
REFERENCES	38
APPENDIX I	41
APPENDIX II	51
APPENDIX III	56
VITA	86
ABSTRACT	87

LIST OF FIGURES

1. Measured electrode potential versus time, 25°C	16
2. Natural logarithm of $m_{\text{Fe}^{3+}}$ versus time, 25°C	23
3. Arrhenius plot	35
4. Example output produced by the program IRON	74
5. Aqueous speciation diagram for ferric iron	76
6. Example output produced by the program REDOX	85

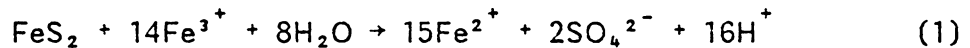
LIST OF TABLES

1. Sample provenance	12
2. Experimental values for the rate constants at 25°C, pH = 2.0 and $m^{\circ}_{\text{Fe}^{3+}} = 10^{-3}$	27
3. Experimental values for the rate constants at 25°C, pH = 2.0 and varying initial ferric iron concentrations	30
4. Experimental values for the rate constants at pH = 2.0, $m^{\circ}_{\text{Fe}^{3+}} = 10^{-3}$ and different temperatures	32
5. 2 θ calculations for powder x-ray diffraction patterns	44
6. DISTN species .list	63

CHAPTER 1

INTRODUCTION

Pyrite is the most abundant of the sulfide minerals and it occurs in nearly all types of geologic environments. Marcasite, the orthorhombic FeS₂ polymorph, is also quite common. Consequently, FeS₂ is encountered in abundance in most mining environments, particularly in coals and in Cu, Pb and Zn sulfide ores. Oxidation of these two minerals by ferric iron is a particularly important natural process because of the acid produced by the reaction:



The sulfuric acid released by this redox reaction produces high levels of acidity in mine drainages. Other environmental systems in which oxidation of iron sulfide minerals and the subsequent release of acid is an important process are supergene alteration of ore deposits, formation of acid sulfate soils, formation of sandstone type uranium and copper deposits, and in situ mining and dump leaching of heavy metals for economic recovery (Nordstrom, 1982).

There are several reasons to suspect that the fundamental reactivities with aqueous ferric iron of pyrite and marcasite from different sources might vary. First, museum grade specimens of both FeS₂ minerals show a marked difference in their susceptibility to oxidation by air (Stokes, 1901). Some samples exhibit varying degrees of surface corrosion while others remain bright and untarnished.

Second, the acid production potential of mine wastes does not always correlate with the abundance and type of FeS_2 in the host rock (Caruccio, 1968, 1970). Third, the mineral pyrite exhibits a wide range of variation in many of its chemical and physical properties (Smith, 1940, 1942). The variation in a specific property can sometimes be correlated with the conditions of formation of the mineral. For example, Rakcheyev and Chernyshev (1968) found that the variation in the band gaps of synthetic pyrites correlates with the temperature of synthesis, the higher the temperature of synthesis the wider the band gap. They also suggest that synthetic pyrite becomes richer in iron but poorer in sulfur with increasing temperature. Natural pyrite specimens exhibit both n- and p-type semiconduction, sometimes within the same crystal (Vaughan and Craig, 1978). Shuey (1975) suggests that natural pyrite formed at low temperatures tends to be p-type (iron deficient, electron acceptors) whereas that formed at higher temperatures tends to be n-type (sulfur deficient, electron donors). However, non-stoichiometry of pyrite is less than 1 atom-percent (Shuey, 1975). Rising (1973) concludes that marcasite is iron-rich relative to pyrite based on his literature review of non-stoichiometry in the two polymorphs. The variation in other properties cannot be correlated with formation conditions. For example, ^{57}Fe Mossbauer parameters of both pyrite and marcasite exhibit appreciable variations which bear no simple relationship to the mineral paragenesis. (Evans. et al., 1982). Rather, in the pyrite crystal lattice the Mossbauer parameters appear to be selectively influenced by impurities, especially

arsenic (Evans, et al., 1982). Other properties of pyrite which are reported to vary significantly are electrical conductivity (Smith, 1940, 1942), semiconducting type (Shuey, 1975), crystal form (Dana, 1944), density (Smith, 1942), optical anisotropism (Stanton, 1957, and Gibbons, 1967), and impurity content (Fleischer, 1955). Thus, if the rate limiting step for reaction 1 depends upon any of the above properties, the reaction rates should vary accordingly.

The purpose of this study is to determine whether pyrite and marcasite specimens from various sources show a significant difference in reactivity with the aqueous ferric ion. The reactivity of each of seven pyrite and three marcasite samples was determined under aerobic conditions by monitoring the change in oxidation-reduction (redox) potential of 500 milliliters of pH 2.0, 10^{-3} molal ferric chloride solution in contact with a one gram sample of pulverized pyrite or marcasite (100-200 mesh) during a 250 minute period. The overall stoichiometry for this reaction as given in equation 1 was verified in studies similar to the present one by Garrels and Thompson (1960) and by Singer and Stumm (1969). The rate of reduction of ferric ion can be used as a measure of the extent of oxidation of the sulfide mineral (Garrels and Thompson, 1960), since 14 moles of ferric iron are reduced during the decomposition of one mole of FeS_2 , releasing one additional mole of iron to the solution. Because this process involves the ferric-ferrous redox reaction, the redox potential (Eh) of the solution as given by the Nernst equation (Nordstrom, et al., 1979):

$$\text{Eh} = \text{E}^\circ + (\text{RT}/\text{nF}) \ln [\text{a}_{\text{Fe}^{3+}} / \text{a}_{\text{Fe}^{2+}}] \quad (2)$$

can be used to measure the kinetics of the reaction. In the Nernst equation, E° is the standard half-cell potential of the ferric-ferrous redox couple, R is the gas constant, T is the temperature in Kelvins, n ($= 1$) is the number of electrons involved in the ferrous-ferric electron transfer, F is the Faraday constant ($96.49 \text{ kJ mol}^{-1}$), and a_i represents the activity of the uncomplexed species (i) in aqueous solution. The concentration of ferric iron can be calculated at each Eh using this equation when activity coefficients and aqueous speciation of the metal ions are taken into account (Kester, et al., 1975).

The experiments were run at low pH to reproduce conditions similar to those found in acid mine drainage. Furthermore, ferric ion hydrolysis and oxidation of ferrous iron is minimized at pH 2 and below. At this pH the activity of the free ferric ion is high compared to the activity of ferric complexes. Speciation calculations were performed by a computer program written for this study (see Appendix III). At these low pH's, the presence of oxygen does not affect the observed rate because the rate of ferric reduction by pyrite is very much greater than the rate of oxidation of ferrous to ferric by O_2 (Singer and Stumm, 1969). Hydrochloric rather than sulfuric acid was used to acidify the solutions in order to avoid any potential interference of sulfate with the oxidation reaction. The initial concentration of ferric in the oxidizing solution for all runs ranged between 10^{-5} and 10^{-3} molal. Berner (1970) reports that dissolved iron concentrations in acidic mine waters (where ferric oxidizes pyrite) can be as high as 100

to 500 ppm (1.79×10^{-3} to 8.95×10^{-3} molal) and pH's are often less than 2. For the majority of the runs, initial ferric concentrations were kept at around 60 ppm (1.03×10^{-3} molal) so the ionic strengths were low enough to apply the extended form of the Debye-Huckel equation for activity coefficient calculations (see Appendix III). At pH's above 3 and total iron concentrations below 10^{-5} molal, the Eh electrode does not respond exclusively to the ferric-ferrous couple in an aerated system (Natarajan and Iwasaki, 1974).

This paper is divided into 6 parts. Following the introduction, a brief discussion of previous related studies is presented in Chapter 2. Chapter 3 contains a description of the experimental materials, apparatus and procedures. In Chapters 4 and 5, respectively, the method of rate constant calculation and a discussion of the experimental results are presented. Finally, the last chapter offers the conclusions that may be drawn from the results.

CHAPTER 2

PREVIOUS STUDIES

Pyrite oxidation has been studied extensively in connection with its role in producing acidic mine drainage. There is a general consensus that in the acid mine drainage environment pyrite is initially oxidized by oxygen to produce ferric hydroxides and sulfuric acid (Nordstrom, 1982). When the pH falls below 4.5, the solubility of ferric iron increases and below pH 2.5 the ferric ion activity becomes significant (Singer and Stumm, 1969 and Kleinmann, et al., 1981) and is maintained by bacterially catalyzed oxidation of ferrous iron to ferric iron. Under these conditions, ferric iron is the oxidant of pyrite. Once the cycle of acid production is established (Singer and Stumm, 1970), low constant pH's are maintained by acid producing reactions (e.g., metal hydrolysis) and acid consuming reactions (e.g., bacterially catalyzed oxygenation of ferrous iron).

Many of the experimental studies on pyrite oxidation deal with the kinetics of aqueous ferrous iron oxidation by dissolved oxygen which appears to be the rate determining step in the overall acid production cycle (Singer and Stumm, 1969). Other studies have examined the effects of water, non-ferric acid solutions, air or pure oxygen on pyrite oxidation. Nordstrom (1982) provides a comprehensive review of this literature. There are fewer studies that directly investigate the kinetics and mechanism of FeS_2 oxidation by the aqueous ferric ion, and none that have examined relative reactivities of a variety of FeS_2 types.

Garrels and Thompson (1960) studied the anaerobic dissolution of three pulverized (100-200 mesh) pyrite specimens from different sources in acid ferric sulfate solutions by measuring solution redox potentials with time over run lengths of 24 to 100 hours. The various pyrites reacted at markedly different rates, but the reaction mechanism appears to have been the same for all specimens. The rates were found to be independent of pH over the interval 0 to 2.0 (Garrels and Thompson, 1960). By plotting the 'average' rate of reduction of ferric iron ($\Delta \text{moles Fe}^{3+} / \Delta \text{time}_{\langle \frac{1}{2} \rangle}$) as a function of initial ferric iron concentration they found that the average rate is independent of initial ferric iron concentration over the range 10^{-5} to 10^{-3} M Fe^{3+} . However, their potential versus logarithm of time plots for 15 runs clearly show decreasing rates with increasing initial concentration of ferric iron. These plots also show that the rates decrease with time and consequently with $m_{\text{Fe}^{3+}}$ which implies direct kinetic dependence on Fe^{3+} . Garrels and Thompson (1960) interpret these results as indicating rate control by an adsorption process in which ferric and ferrous ions compete for surface adsorption sites. They assume that the rates are proportional to the fraction of the pyrite surface occupied by ferric ions, and thus to the fraction of ferric iron to total iron present in the solution. The actual dissolution mechanism is described in general terms by these authors as oxidation of pyrite to ferrous ions and sulfate ions only at those sites occupied by ferric ion, this process being slow relative to adsorption.

Based on Garrels and Thompson's results (1960) and results from their own experiments, Smith, et al. (1968) postulate a mechanism consisting of four elementary reactions with electron transfer from the solid to an adsorbed ferric species as the rate-controlling step. They use an adsorption model to derive a rate equation from which they calculate adsorption equilibrium constants for ferrous and ferric iron using their experimental kinetic data. Values of their calculated adsorption equilibrium constants suggest that the aqueous ferrous ion is preferentially and more strongly adsorbed onto the pyrite surface than the aqueous ferric ion. Their data plots show that the oxidation rate decreases with decreasing ferric-ferrous ratio. Smith, et al. (1968), performed their experiments at pH 0.2 and constant potential using varying ferric/ferrous ratios in one series of runs and varying initial ferric concentrations from 10^{-4} to 10^{-2} M in another series of runs.

In experiments similar to those of Garrels and Thompson (1960), Singer and Stumm (1969) found virtually no difference between the rates of reduction of Fe^{3+} by pyrite under aerobic or anaerobic conditions. They varied both initial ferric iron concentrations (10^{-4} to 10^{-3} M ferric perchlorate) and pyrite concentrations (0.5 to 5 gram of 200-250 mesh FeS_2 /liter solution) at pH 1.0 with run lengths of approximately 500 minutes. These authors verify the stoichiometry of equation 1 by noting a 7% increase ($15/14=1.07$) in the concentration of total dissolved iron. Because the rate of oxidation is independent of pH below 2.0, Singer and Stumm (1969) suggest a simple rate law

dependent upon the concentrations of the two reactants, of the form:

$$-d \text{Fe}^{3+}/dt = k[\text{Fe}^{3+}]^m[\text{FeS}_2]^n$$

where $[\text{FeS}_2]$ actually represents the pyrite surface area to mass of solution ratio (A/M). Using the integrated form of their rate equation, plots of their data indicate a first order dependence in both pyrite concentration (A/M) and ferric iron concentration ($m, n = 1$) (Singer and Stumm, 1969). However, they note that the rate constants increase with decreasing initial concentration of ferric iron, implying an inverse dependence of the rate on ferric iron, similar to Garrels and Thompson's results (1960).

The complex and often conflicting results of previous studies are a result of the wide range of possible reaction mechanisms. Clark (1966) defends the case for an electrochemical mechanism versus simple dissolution by citing the facts that pyrite conducts electricity, exhibits potentials in aqueous solutions, and is very insoluble. This complicates the matter even further, since the 6-electron difference in oxidation states between sulfur in pyrite and that in sulfate can be obtained by one or at most two electron transfers per reaction (Basalo and Pearson, 1967 and Nordstrom, 1982). Any one of these multiple oxidation steps could be rate-limiting.

At low pH values ferric iron oxidizes pyrite much more rapidly than molecular oxygen does (see Nordstrom's Figure 1, 1982). This significant increase in reaction rates when ferric ion is involved suggests that a ferric species directly attacks the pyrite surface and that the mechanism should be described in terms of a heterogeneous

reaction. A specific electrochemical interaction between ferric ion and pyrite through the solution/solid interface appears to be the rate determining step.

CHAPTER 3

EXPERIMENTAL

Pyrite and marcasite samples from various localities were examined in polished section under reflected light and by powder x-ray diffraction to determine their suitability for reactivity experiments (see Appendix I). Only pure pyrite and pure marcasite samples were selected as run material. These samples are listed in Table 1 along with the available information on their geologic origin.

Run solids were prepared prior to each experiment by comminution in a Tekmar Model A10 Analytical Mill. The pulverized sample was then dry sieved to isolate the 100-200 mesh (75-150 micron) size fraction. A 1.0000 ± 0.0005 gram sample of this material was used in each run.

Run solutions were prepared by combining the appropriate volume of 75% $\text{FeCl}_3 \cdot 6\text{H}_2\text{O}$ reagent solution with 1 liter distilled/deionized H_2O previously acidified to pH 2.0 with 1.5 milliliters concentrated HCl. Five hundred milliliters of the freshly prepared solution was used for each run. Solution pH was checked before and after each run using an Orion Research Microprocessor pH/millivolt meter Model 811 with an Orion Research pH electrode. The final pH of the run solutions was always within 0.04 pH units of the initial pH of 2.00. The concentrations of ferrous and total iron in the initial and final run solution of each experiment were determined spectrophotometrically using 1,10-phenanthroline following the procedure of Harvey, et al. (1955) with minor modifications. Ferric iron was determined by

TABLE 1

Sample Provenance

Sample Number	Locality	Type of deposit crystal habit.
<u>LOWER TEMPERATURE EARLY DIAGENETIC PYRITES</u>		
PY-01	Kentucky	Concretion in coal underclay; framboidal and microcrystalline cubic
PY-02	Napoleon Quarry, Indiana	Concretion in dolomitized Silurian carbonate; microcrystalline cubic
PY-05	Illinois	Sand dollar concretion in coal; fibrous
<u>HIGHER TEMPERATURE PYRITES</u>		
PY-04	Renseleer Quarry, Indiana	Hydrothermal vug filling in dolomitized limestone; crystalline, massive
PY-06	Illinois-Wisconsin Pb-Zn District, Schullsburg, Wisconsin	Hydrothermal vug filling; crystalline, massive, distorted cubes
PY-10	Pennsylvania	Metamorphic; single cubic crystals in schist
PY-11	Pas-de-Calais, Northern France	Radial fibrous crystals in a compact globular concretion
<u>HYDROTHERMAL MARCASITES</u>		
MC-01	Illinois-Wisconsin Pb-Zn District Schullsburg, Wisconsin	Vug filling associated with sphalerite and calcite; cockscomb
MC-02	Renseleer Quarry, Indiana	Vug filling; cockscomb
MC-03	Tri-State District, Joplin, Missouri, Jasper Co., Dana locale	Associated with galena and calcite; cockscomb

difference (see Appendix II for iron assay procedure). Solutions were assayed at selected intervals during a run by extracting 5 ml aliquots. Each of these samples was filtered through a 0.8 micron Millex-PF Millipore filter to remove suspended pyrite grains before analysis.

The experiments were performed in a constant temperature water bath employing a mercury relay temperature control which held temperatures constant to $\pm 0.3^{\circ}\text{C}$. Cold tap water was circulated through cooling coils in the water bath to maintain 25°C temperatures. A 500 ml Kimax reaction kettle containing the run solution was lowered into the bath and held in place by a plexiglass cover. A glass impeller mounted on an overhead stirring assembly was lowered into the solution through a non-air-tight access port in the cover. The standard stirring rate was set at 700 rpm which was sufficient to create a vortex in the solution and to suspend most of the run material. The coarsest material remained in motion along the bottom of the reaction vessel. This overhead stirring apparatus eliminated abrasion of the solid particles encountered when using a teflon-coated magnetic stir bar and the electrically powered motor permitted better control over the stirring rate than air or water driven magnetic stirrers. A Fisher combination platinum/saturated KCl/Ag-AgCl electrode was used to measure redox potentials of the run solutions. The electrode was immersed in the solution through a second access port in the cover and the solution was brought to run temperature. The 1.0 gram charge of run material was added to the run solution through the impeller access port after potential readings had stabilized, approximately 10 minutes after the

beginning of each run. The potential readings were monitored during each run by an Apple II Plus microcomputer with Disk II Operating System via an Interactive Microware Adalab interface card. The one hundred readings taken at constant intervals during the course of each run were recorded by an Epson MX-80 printer. Results for a typical run are shown in Figure 1. Standard run length was 250 minutes.

The potential produced by the combination platinum/saturated KCl/Ag-AgCl reference electrode was subsequently adjusted to give the Eh, i.e., the reduction-oxidation potential relative to the standard hydrogen electrode (SHE). For the AgCl reference electrode used here, this correction consisted of adding the half cell potential (E_s') of the reference electrode to the measured solution potential (emf) (Langmuir, 1971):

$$E_h = \text{emf}(\text{measured}) + E_s' \quad (3)$$

The half-cell potential of the reference electrode is given by:

$$E_s' = E_c + E_j \quad (4)$$

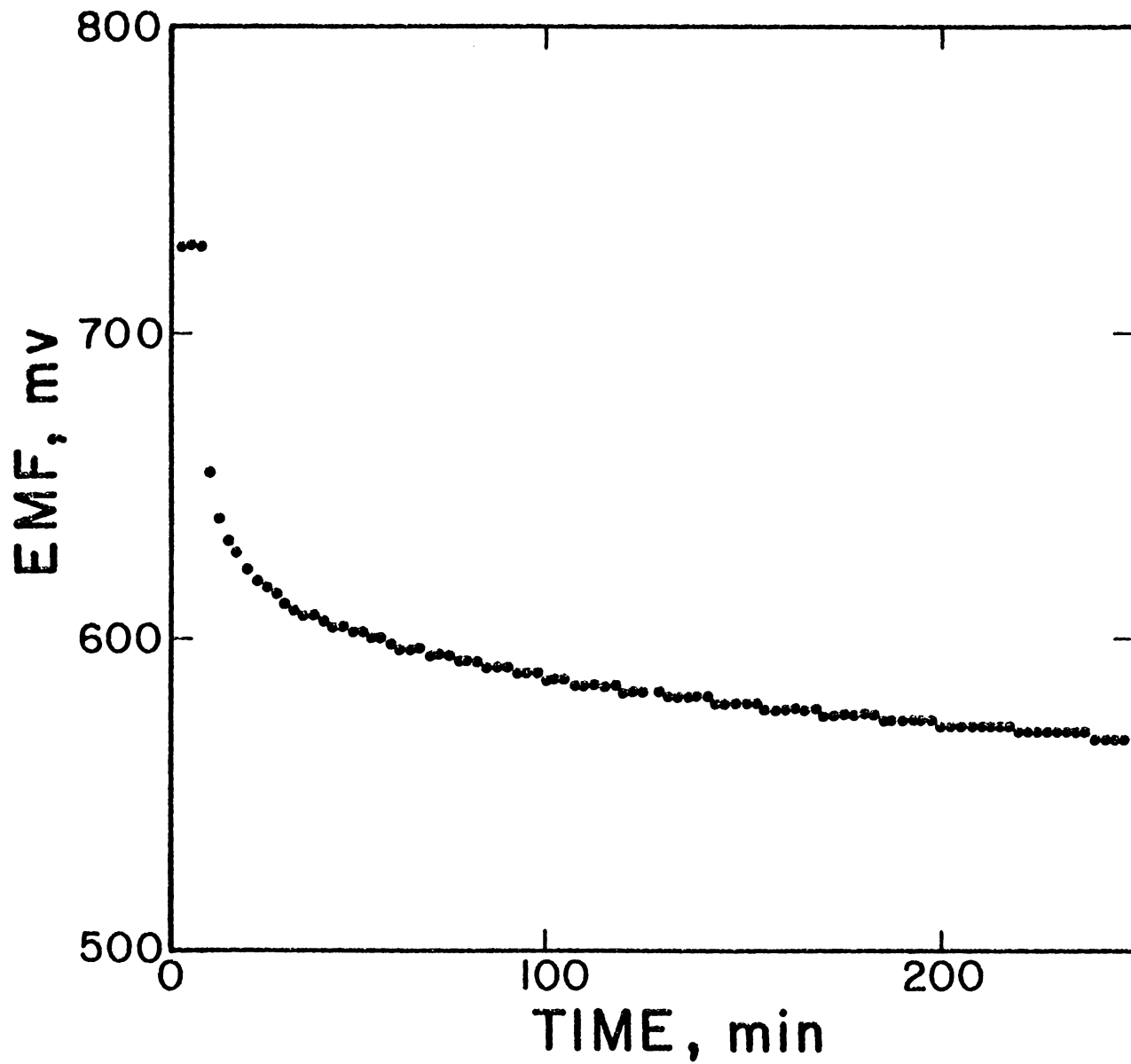
(Langmuir, 1971) where E_c is the potential due to the reference half-cell reaction:



and E_j is the liquid junction potential.

Zobell's solution (Langmuir, 1971) was used as a redox potential buffer to check the combination Eh electrode system for proper response and to measure the calibration for the platinum electrode-reference electrode combination. The emf of Zobell's solution measured

Figure 1: Plot of emf (measured in millivolts) versus time (in minutes) for a typical run (25°C , $m^{\circ}_{\text{Fe}^{3+}} = 10^{-3}$, $\text{pH} = 2.0$, PY-04-R16). The stepwise appearance of the data points on this plot is due to digitization of the potential readings by the computer analog to digital converter.



with a platinum electrode referenced against a saturated KCl/Ag-AgCl electrode is given by the temperature dependent equation determined by Nordstrom (1977):

$$\text{emf}(Z) = 0.23145 - 1.5220 \times 10^{-3}(T-25) - 2.2449 \times 10^{-6}(T-25)^2 \quad (6)$$

where T is the temperature in degrees Celsius and the emf is in volts. Potentials measured at 25°C with the combination Eh electrode were less than the potentials calculated from equation 6 by 0.004v. The Eh, Eh(Z), of Zobell's solution relative to the SHE is given by the following equation (Nordstrom, 1977):

$$\text{Eh}(Z) = 0.43028 - 2.5157 \times 10^{-3}(T-25) - 3.7979 \times 10^{-6}(T-25)^2 \quad (7)$$

Using equations 6 and 7 the half-cell potential correction (E_s') can be calculated from equation 3, thus:

$$\text{Eh}(Z) - \text{emf}(Z) = E_s' = 0.19883\text{v at } 25^\circ\text{C}. \quad (8)$$

Subtracting the constant potential difference of 0.004v measured by the combination Eh electrode gives $E_s' = 0.19483\text{v}$. The Eh was, thus, calculated from the measured emf by

$$\text{Eh}(\text{volts}) = \text{emf}(\text{measured, volts}) + 0.19483. \quad (9)$$

Ferric iron concentrations calculated from these Eh values using the Nernst equation, taking into account activity coefficients and speciation, agree well with concentrations determined spectrophotometrically.

Surface areas of the run materials were determined after the experiments by the five-point BET method using a Quantachrome Quantasorb. The 2.5-3.5 gram samples were heated to 100°C for 2-3 hours during initial degassing. Argon was used as the adsorbate gas

with helium as carrier.

CHAPTER 4

CALCULATION OF THE RATE CONSTANTS

The experimental data are best fit by a rate law that is first order in ferric iron and that accounts for the ratio of the surface area of reacting solid to mass of solution:

$$-d m_{\text{Fe}^{3+}} / dt = r = k (A/M) m_{\text{Fe}^{3+}} \quad (10)$$

where k is the rate constant and $m_{\text{Fe}^{3+}}$ is the molal concentration of free (uncomplexed) ferric iron. A is the relative interfacial area between the solid and the aqueous phase, M is the relative mass of water in the system, and (A/M) represents the extent of the system where the standard system is 1.0 m² interfacial area per 1.0 kg solution as defined by Rimstidt (1980). Combining the constants k and (A/M) into an apparent rate constant, k' , the integrated form of this rate law:

$$\ln m_{\text{Fe}^{3+}} = k't + \ln m_{\text{Fe}^{3+}}^{\circ} \quad (11)$$

shows that a plot of $\ln m_{\text{Fe}^{3+}}$ versus time should yield a straight line with slope k' and intercept $\ln m_{\text{Fe}^{3+}}^{\circ}$. The surface area of reacting solid per unit mass is assumed constant because of the small extent of reaction over the four hour run period.

The ferric iron concentration at each time, t , was calculated from the solution potential using the Nernst relation as given in equation 2. At 25°C, $E^{\circ} = 0.771$ volts and $RT/F = 0.02569$ volts so the Nernst equation can be written:

$$\exp[(Eh-0.771)/0.02569] = a_{\text{Fe}^{3+}} / a_{\text{Fe}^{2+}} \quad (12)$$

and

$$a_{\text{Fe}^{3+}} / a_{\text{Fe}^{2+}} = (\gamma_{\text{Fe}^{3+}} m_{\text{Fe}^{3+}} / \gamma_{\text{Fe}^{2+}} m_{\text{Fe}^{2+}}). \quad (13)$$

Setting the quantity in brackets equal to X and defining $m_{\text{Fe}^{2+}} = m^{\circ}_{\text{Fe}^{3+}} - m_{\text{Fe}^{3+}}$ gives:

$$\exp X = (\gamma_{\text{Fe}^{3+}} / \gamma_{\text{Fe}^{2+}}) [m_{\text{Fe}^{3+}} / (m^{\circ}_{\text{Fe}^{3+}} - m_{\text{Fe}^{3+}})]. \quad (14)$$

In our experiments $m^{\circ}_{\text{Fe}^{3+}}$ is the initial concentration of ferric iron which is equal to the initial total iron concentration. To correct for the amount of iron released from the pyrite over the course of the run, the stoichiometry of equation 1 is assumed such that for every 14 moles of ferric iron reduced there is one additional mole of ferrous iron released from pyrite. This causes a 7% increase in $m_{\text{Fe}^{2+}}$ over that calculated from $m^{\circ}_{\text{Fe}^{3+}} - m_{\text{Fe}^{3+}}$. The equation then becomes

$$\exp X = \gamma(R) [m_{\text{Fe}^{3+}} / 1.07(m^{\circ}_{\text{Fe}^{3+}} - m_{\text{Fe}^{3+}})] \quad (15)$$

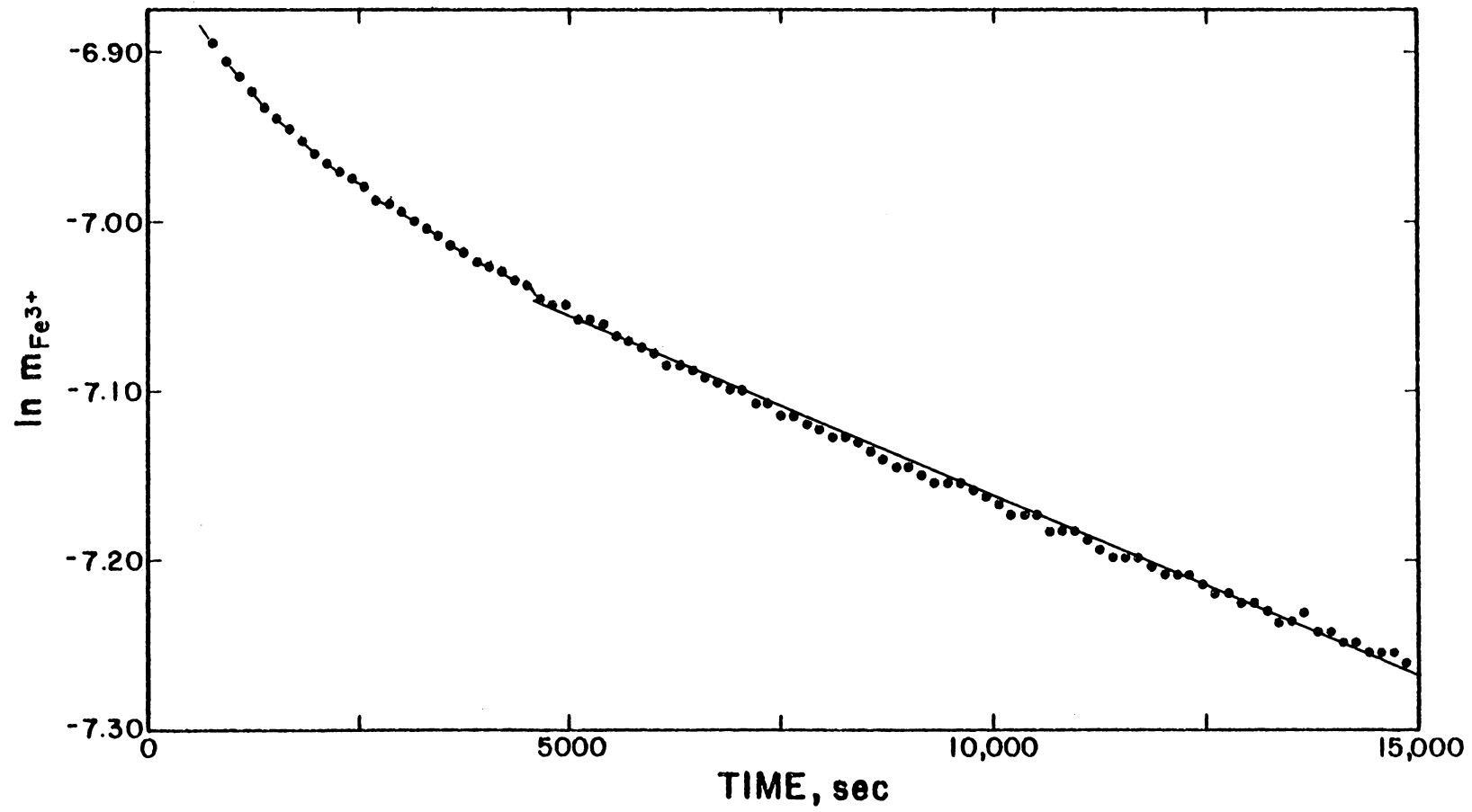
where $\gamma(R) = \gamma_{\text{Fe}^{3+}} / \gamma_{\text{Fe}^{2+}}$ and is defined as the total stoichiometric activity coefficient ratio for ferric/ferrous. A computer program coded to calculate the distribution of aqueous species and ferric-ferrous redox equilibria in the experimental solutions provided values for $\gamma(R)$ (see Appendix III). Solving for $m_{\text{Fe}^{3+}}$:

$$m_{\text{Fe}^{3+}} = m^{\circ}_{\text{Fe}^{3+}} [\exp X / ((\gamma(R)/1.07) + \exp X)]. \quad (16)$$

The reactivity of each sample was determined at 25°C and pH = 2.0 using initial ferric iron concentrations of 10^{-3} molal. Plots of $\ln m_{\text{Fe}^{3+}}$ (calculated using equation 16) versus time for each of the runs show an

initial steep slope (Figure 2). As the run progresses, the rate of decrease of the ferric iron concentration slows down to produce a linear plot of $\ln m_{\text{Fe}^{3+}}$ versus time. Three factors which may contribute to the initial sharp decrease in potential (decrease in ferric iron relative to ferrous iron) are (1) rapid dissolution of fine particles of FeS_2 adhering to the freshly prepared surface and/or dissolution of a disturbed surface layer, (2) rapid adsorption of ferric iron onto reactive sites at the solid surface, and (3) rapid decrease and disappearance of a streaming potential at the platinum electrode produced by the relative movement of electrode and solution due to stirring. Streaming potentials were measured in solutions of different ferric/ferrous ratios. In solutions having very large ferric/ferrous concentration ratios, the streaming potential is highest (50 mv). Upon addition of a minute amount of ferrous iron, the streaming potential drops dramatically and then disappears as the ferric/ferrous concentration ratio drops below about 30. Iron determinations on the run solutions immediately following the addition of pyrite show that the ferric/ferrous ratio reaches a value well below 30 within a short period of time after beginning the run, i.e., within 10 or 20 minutes. It was difficult to separate the effects of adsorption from those of dissolution of fine powder or disturbed surface using our experimental method. Adding more ferric iron to a run that was half completed did not produce the steep initial decrease seen at the beginning of the runs. Rather, the potential increased but the slope remained essentially the same as the previous linear portion. The rapid initial decrease in the

Figure 2: Plot of $\ln m_{\text{Fe}^{3+}}$ versus time (in seconds) for a typical run (25°C , $m^{\circ}_{\text{Fe}^{3+}} = 10^{-3}$, $\text{pH} = 2.0$, PY-04-R16, $k' = 2.09 \times 10^{-5}$). Experimental points calculated from Eh using equation 16 in text. The first data point, plotted at $t = 750$, is the first reading after addition of run material to run solution at $t = 600$. Solid line indicates the best fit straight line found by a linear regression of the data from $t = 4500$ to $t = 15000$, $r^2 = 0.997$. Dashed line indicates initial steep slope caused by the combined effects of rapid dissolution of fine FeS_2 particles and/or a disturbed surface layer, adsorption, and streaming potentials.



ferric/ferrous ratio in our experiments is probably due to a combination of the above effects. The effects of these factors on the reaction rates were eliminated by excluding the first 75 minutes of potential readings from the data analysis.

In order to calculate the rates of higher temperature runs, values for the reference electrode potential (E_s'), the standard potential for the ferric-ferrous couple (E°), and the total stoichiometric activity coefficient ratio ($\gamma(R)$) at the various temperatures were required. Langmuir (1971) lists E_s' values for Ag-AgCl reference electrodes from 0 to 50°C in his Table 4. The values listed there were adjusted according to the difference between our E_s' value at 25°C and Langmuir's value. This consisted of subtracting (0.19483) from Langmuir's value (0.1985) to obtain a difference of -0.00367. At each of the temperatures of interest, 0.00367 was added to Langmuir's value to obtain the appropriate E_s' value used in our calculations. Whittemore and Langmuir (1972) determined an empirical temperature function for standard electrode potentials (E°) for the ferric-ferrous couple:

$$E^\circ(T) = -1.23 \times 10^{-2} + 4.147 \times 10^{-3}T - 5.111 \times 10^{-6}T^2 \quad (17)$$

where T is in Kelvins. This function was used to calculate the E° values at the various temperatures of the runs. The total stoichiometric activity coefficient ratio for each temperature above 25°C was estimated from Whittemore and Langmuir's (1972) data by plotting the ratio $\gamma_{Fe^{3+}}/\gamma_{Fe^{2+}}$ (calculated from their Debye-Huckel activity coefficients values) as a function of temperature, fitting a straight line,

and then drawing a line of the same slope through our $\chi(R)$ value at 25°C. Values for $\chi(R)$ at the various temperatures were taken from this plot.

CHAPTER 5

DISCUSSION OF RESULTS

Table 2 lists the rate constants calculated by linear regression of the experimental data at 25°C, pH = 2.0, and $m^{\circ}_{\text{Fe}^{3+}} = 10^{-3}$. The coefficients of determination, r^2 , for the regression fits for all the runs were ≥ 0.989 and the mean standard error of the slope k' was 1.7×10^{-7} . The rate constant, k , in units of sec^{-1} , was obtained by dividing the slope k' of the $\ln m_{\text{Fe}^{3+}}$ versus time plot by (A/M) . The samples are divided into three groups: low temperature/early diagenetic pyrites, higher temperature pyrites, and marcasites. The mean values of the rate constant, k , for each of the 3 groups are: $9.91 \times 10^{-5} \text{ sec}^{-1}$ for low temperature/early diagenetic pyrite, $26.98 \times 10^{-5} \text{ sec}^{-1}$ for higher temperature pyrite, and $15.46 \times 10^{-5} \text{ sec}^{-1}$ for marcasite. Table 2 also lists the BET measured surface areas and the calculated (A/M) . The error on the surface areas measured by the five-point BET method is within $\pm 5\%$ (Lowell, 1979). By propagation of errors on k' and A , the overall error on the rate constant, k , becomes about $\pm 5\%$. Comparing the values of k' , (A/M) , and k (Table 2) for the high and low temperature pyrites shows that it is the greater BET measured surface area of the early diagenetic type (by a factor of 10) that allows the same mass of FeS_2 to react much more quickly than the higher temperature pyrites which have a lower BET measured surface area. It

TABLE 2

Experimental values for the rate constants
at 25°C, pH = 2.0 and $m^{\circ}_{\text{Fe}^{3+}} = 10^{-3}$

Run Number	$k' \times 10^5$ (a)	Surface Area (b)	A/M (c)	$k \times 10^5$ (d)
<u>LOW-TEMPERATURE/EARLY DIAGENETIC PYRITES</u>				
PY-01-R1	8.71			14.21
PY-02-R1	5.55	0.3065	0.6130	9.05
PY-05-R1	3.96			6.46
<u>HIGHER TEMPERATURE PYRITES</u>				
PY-06-R1	1.69			22.82
PY-10-R1	1.74	0.0370	0.0740	23.50
PY-11-R1	2.26			30.54
PY-04-R11	1.49			24.03
PY-04-R16	2.09		0.0620	33.76
PY-04-R24	1.48	0.0310		23.89
PY-04-R34	1.66			26.74
PY-04-R23	3.79		0.1240	30.56
<u>MARCASITES</u>				
MC-01-R1	1.16			15.86
MC-01-R2	1.31	0.0367	0.0734	17.90
MC-02-R1	1.01			13.75
MC-03-R1	1.05			14.33

- (a) k' = slope of $\ln m_{\text{Fe}^{3+}}$ versus time plot.
- (b) BET measured surface area in units of $\text{m}^2 \text{g}^{-1}$. Run material was mixed to obtain sufficient sample mass for BET method in the following manner: PY-01 + PY-02 + PY-05 for low temp. pyrites; PY-06 + PY-10 + PY-11 for higher temp. pyrites; PY-04 for higher temp. pyrites; MC-01 + MC-02 + MC-03 for marcasites.
- (c) $A^{\circ} = 1 \text{ m}^2$ and $M^{\circ} = 1 \text{ kg}$, as defined by Rimstidt (1980).
- (d) k is in units of sec^{-1} .

is, therefore, essential to use measured values for specific surface areas rather than values calculated from grain sizes for calculating rate constants from experimental kinetic data. Given the $\pm 5\%$ error, the mean value for the rate constants for each of the three groups is statistically distinct. This distinction in rates is probably significant in terms of the detailed chemistry of the reaction mechanism. For example, if the rate-determining step is electrochemical, these minor differences in reactivity may reflect the influence of semiconductor type. However, in terms of geological processes, this distinction is not justifiable because the mean rates are well within half an order of magnitude. Geologically, then, the fundamental reactivities of bulk solid marcasite and all bulk solid pyrites do not differ appreciably.

The absolute rate values calculated for the low temperature pyrites are in question due to a problem with the measured surface area. In order to obtain a sufficient sample mass to make a reasonably accurate surface area measurement, the final run materials from the three low temperature pyrites were mixed. The larger k' for PY-01 suggests that it has a significantly higher specific surface area than the other two, whose k' 's are much lower. Microscopic examination of polished sections prove this to be a reasonable interpretation. The texture of PY-01 is dominantly cryptocrystalline framboidal, PY-02 is microcrystalline cubic with abundant cracks and voids within the individual crystals, and PY-05 consists of much larger, elongate, more homogeneous grains. The BET-measured surface area is probably too low for PY-01 and too high for PY-02 and PY-05. Correcting for this (i.e., using separately

measured surface areas for each sample) would lower the rate constant for PY-01 and increase those for PY-02 and PY-05, probably bringing them into closer agreement. Another problem with the measured rate constants for the lower temperature pyrites lies with the difficulty in preparing an absolutely pure run sample. Because the pyrite grain size in some concretionary aggregates, especially framboidal aggregates, is smaller than the selected grain size of the pulverized run material, complete separation of organic or silicate impurities from the run sample is impossible. This results in a measured surface area of reacting solid that is too high and a rate constant that is too low. Presence of adsorbed impurities (particularly organics) on the surface of the pyrite may inhibit the reaction, also resulting in reaction rate constants that are too low. However, even if the apparent difference in reactivity between higher and lower temperature pyrites is real, and not an artifact of limitation due to systematic errors, the difference is small enough to be accounted for by the above mentioned factors.

Table 3 lists the rate constants determined at 25°C and pH = 2.0 for samples of a standard pyrite, PY-04, at different initial ferric iron concentrations. The rate constants increase with decreasing initial ferric iron concentration implying an inverse dependence of the rate on ferric iron. These results are similar to the findings of Singer and Stumm (1969). Garrels and Thompson's (1960) plots of Eh versus $\log_2 t$ also show this trend. Plots of the rate constants from this study versus $m^\circ_{\text{Fe}^{3+}}$ and versus the square root of the initial ionic strength of the solution are not linear. A linear plot would indicate that the

TABLE 3

Experimental values for the rate constants
at 25°C, pH = 2.0, and varying initial ferric iron concentrations
for a standard pyrite (PY-04)

Run Number	$m^{\circ}\text{Fe}^{3+}\times 10^4$	$k'\times 10^5$	$k\times 10^5$
PY-04-R18	3.94	3.88	62.53
PY-04-R21A	4.83	2.92	47.18
PY-04-R20	8	1.66	26.73
PY-04-R21B	8.41	1.91	30.77
PY-04	10.02	1.68	27.10
PY-04-R22	42.79	0.87	14.02

apparent inverse dependence of the rate on ferric iron is an ionic strength effect. Since the rate law relates the rate constant to ferric iron concentration, this apparent inverse dependence of rates on initial ferric iron concentration may be an artifact. However, the reaction mechanism may change with total iron concentration.

Activation Energy - Temperature Dependence of the Reaction Rate

The temperature dependence of the reaction rate constant is given by the Arrhenius equation:

$$k = (A') \exp (-E_a/RT) \quad (18)$$

where A' is a "preexponential" or "frequency" factor (not to be confused with the surface area A) related to the geometry of the activated complex. E_a is the activation energy of the reaction and represents an energy barrier that must be overcome by the reactants for the reaction to occur. An equivalent form of the Arrhenius equation is:

$$\ln k = (-E_a/R)(1/T) + \ln (A') \quad (19)$$

so a plot of $\ln k$ versus $1/T$ should yield a straight line with slope $-E_a/R$, if the reaction mechanism is unchanged over the temperature range of interest. A' can have a slight temperature dependence, but within the experimental error of most measured activation energies, it can for all practical purposes be considered a constant. The activation energy can be calculated from the slope of an Arrhenius plot.

Table 4 lists the rate constants determined using 2 different

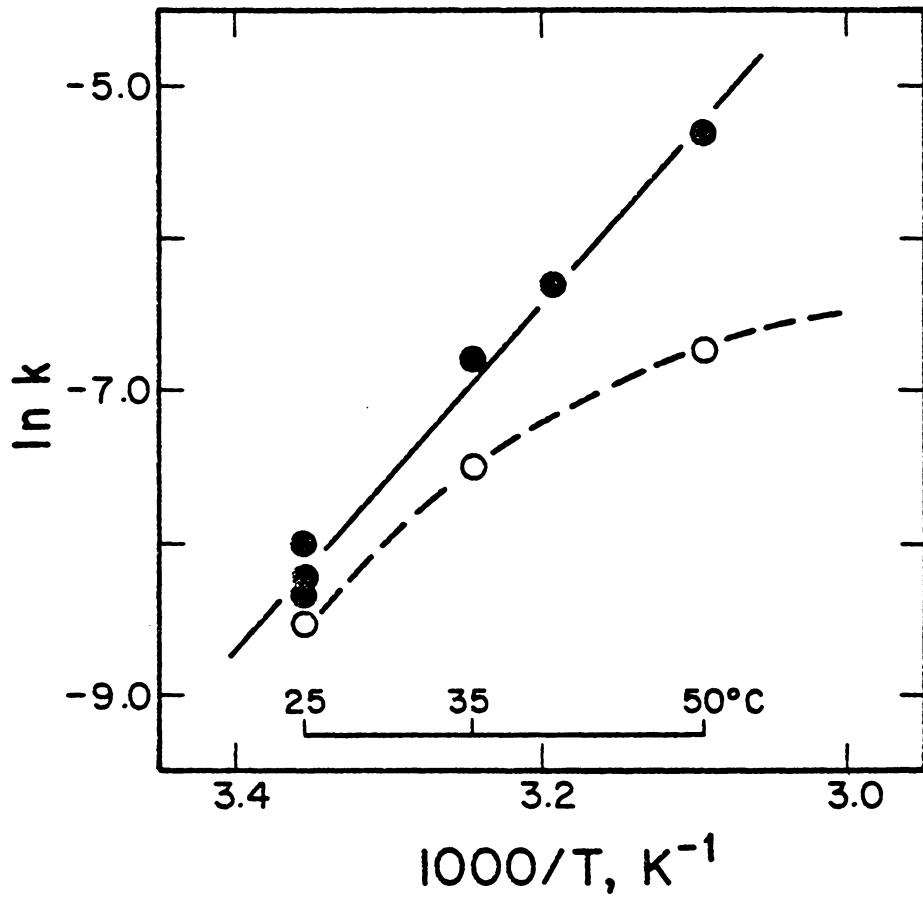
TABLE 4

Experimental values for the rate constants
 at pH = 2.0, $m^{\circ}_{\text{Fe}^{3+}} = 10^{-3}$ and different temperatures
 for a standard pyrite (PY-04)

Run Number	T°C	k'x10 ⁵	kx10 ⁵	ln k
STIRRING RATE = 400 rpm				
PY-04-R10	25	1.23	19.87	-8.52
PY-04-R15	35	3.39	54.68	-7.51
PY-04-R8	50	7.38	119.10	-6.73
STIRRING RATE = 700 rpm				
PY-04-R11	25	1.49	24.03	-8.33
PY-04-R16	25	2.09	33.76	-7.99
PY-04-R24	25	1.48	23.89	-8.34
PY-04-R34	25	1.66	26.74	-8.23
AVERAGE	25	1.68	27.10	-8.21
PY-04-R13	35	6.92	111.56	-6.80
PY-04-R14	40	11.24	181.24	-6.31
PY-04-R9	50	30.32	489.10	-5.32

stirring rates at temperatures from 25 to 50°C and at $m^{\circ}_{\text{Fe}^{3+}} = 10^{-3}$, pH = 2.0, for the standard pyrite, PY-04. Figure 3 is an Arrhenius plot of the rate constants at two different stirring rates. For a stirring rate of 700 rpm, the activation energy is 92 kJ mol⁻¹ (22 kcal mol⁻¹). The initial slope at the slower stir speed is approximately equivalent to this, but at higher temperatures the slope changes to give a limiting activation energy of about 25 kJ mol⁻¹ (6 kcal mol⁻¹). The curvature in the plot for the slower stirring rate is due to temperature dependent activation energies which indicate a change in rate control from surface reaction control at lower temperatures to diffusion (solution transport) control at higher temperatures. The constant activation energy of 92 kJ mol⁻¹ at the faster stirring rate indicates that a surface reaction controls the rates over the entire temperature range of 25 to 50°C. This relatively high activation energy for pyrite oxidation suggests that the rate-determining step for this reaction is the breaking of relatively strong covalent bonds at the solid surface. The fact that a surface chemical reaction controls the rate of pyrite oxidation emphasizes the importance of incorporating the measured surface area to mass of solution ratio when calculating the rate constants.

Figure 3: Arrhenius plot for runs at $m^{\circ}_{\text{Fe}^{3+}} = 10^{-3}$, pH = 2.0, using the standard pyrite, PY-04. Solid circles for runs at stirring rate = 700 rpm. Open circles for runs at stirring rate = 400 rpm. Solid line is best fit line by linear regression of data at stirring rate of 700 rpm ($r^2 = 0.987$). Dashed line indicates trend of $\ln k$ versus $1000/T$ plot for the slower stirring rate.



CHAPTER 6

CONCLUSIONS

The relative reactivities of 3 marcasite and 7 pyrite specimens from various sources were determined in acid ferric chloride solutions. The experimental kinetic data are best fit by a rate law that is first order in ferric iron and that accounts for the surface area of reacting solid to mass of solution ratio (A/M) of the system. The run samples were divided into three groups of FeS₂ types: lower-temperature/early diagenetic pyrite, higher-temperature/hydrothermal and metamorphic pyrite, and hydrothermal marcasite. Mean values for the experimental rate constants for these three groups are $9.91 \times 10^{-5} \text{ sec}^{-1}$, $26.98 \times 10^{-5} \text{ sec}^{-1}$, and $15.46 \times 10^{-5} \text{ sec}^{-1}$, respectively, $\pm 5\%$. On the basis of these mean values the relative reactivities of the three groups are chemically distinct, decreasing in the order higher temperature pyrite greater than marcasite greater than lower temperature pyrite. Geologically these relative differences are too small to account for the great differences in acid production potentials of mine wastes. However, two additional factors must be considered. First, at higher pH's where O₂ oxidation is most important, there still may be a significant difference in reactivities. Second, the specific surface area of early diagenetic pyrite is an order of magnitude greater than that for pyrite from higher temperature deposits. This greater specific surface area allows a given mass of sized material to react more quickly than an equivalent

mass of sized higher temperature pyrite, because the reaction rate is directly proportional to the surface area of the solid exposed to a unit mass of solution. This illustrates the importance of incorporating measured surface area values into the rate constant calculations.

The rate limiting mechanism for oxidation of pyrite by the aqueous ferric ion was found to be a surface (chemical) reaction under the experimental conditions of this study. The activation energy obtained for a standard hydrothermal pyrite from an Arrhenius plot is 92 kJ mol^{-1} (22 kcal mol^{-1}) over the temperature range 25 to 50°C . However, under unstirred conditions, especially at temperatures above 25°C , the rate is likely to be limited by mass transport rates in the solution.

REFERENCES

- Basalo F. and Pearson R. G. (1967) Mechanisms of Inorganic Reactions: A study of metal complexes in solution. 2nd ed. Wiley, New York, 701 pp.
- Berner R. A. (1970) Low Temperature Geochemistry of Iron, Section 26. In Handbook of Geochemistry, 11-1. Springer-Verlag, Berlin.
- Caruccio F. T. (1968) An evaluation of factors affecting acid mine drainage production and the ground water interactions in selected areas of Western Pennsylvania. In Second Symp. Coal Mine Drainage Res., 107-151. Pittsburgh.
- Caruccio F. T. (1970) The quantification of reactive pyrite by grain size. In Third Symp. Coal Mine Drainage Res. Preprints, 123-131. Pittsburgh.
- Clark C. S. (1966) Oxidation of coal mine pyrite. J. Sanit. Eng. Div. Am. Soc. Civ. Eng., 92 Proc. Paper 4802, 127-145.
- Dana D. W. (1944) The System of Mineralogy, Vol. I. Elements, Sulfides, Sulfosalts, Oxides. 2nd ed. Wiley, New York.
- Evans B. J., Johnson R. G., Senftle F. E., Cecil C. B., and Dulong F. (1982) The ^{57}Fe Mossbauer parameters of pyrite and marcasite with different provenances. Geochim. Cosmochim. Acta 46, 761-775.
- Fleisher M. (1955) Minor elements in some sulfide minerals. Econ. Geol. Fiftieth Anniv. Vol., 970-1024.
- Garrels R. M. and Thompson M. E. (1960) Oxidation of pyrite by iron sulfate solutions. Am. Jour. Sci. 258-A, 57-67.
- Gibbons G. S. (1967) Optical anisotropy in pyrite. Amer. Min. 52, 359-370.
- Harvey A. E., Smart J. A., Amis E. S. (1955) Simultaneous spectrophotometric determination of iron (II) and total iron with 1,10-Phenanthroline. Anal Chem. 27, 26-29.
- Kester D. R., Byrne R. H., Liang Y. J. (1975) Redox reactions and solution complexes of iron in marine systems. In Marine Chemistry in the Coastal Environment (ed. T. M. Church), pp. 56-79. Am. Chem. Soc. Symp. Series 18. Washington D. C.
- Kleinmann R. L. P., Crerar D. A. and Pacelli R. R. (1981) Biogeochemistry of acid mine drainage and a method to control acid formation. Mining Engineering. March, 300-305.

- Langmuir D. (1971) Eh-pH determination. In Procedures in Sedimentary Petrology (ed. R. E. Carver), Chapter 26, 597-635. Wiley, New York.
- Lowell S. (1979) Introduction to Powder Surface Area. Wiley, New York, 199 pp.
- Natarajan D. A. and Iwasaki I. (1974) Eh measurements in hydro-metallurgical systems. Minerals Sci. Eng. 6, 35-44.
- Nordstrom D. K. (1977) Thermochemical redox equilibria of ZoBell's Solution. Geochim. Cosmochim. Acta 41, 1835-1841.
- Nordstrom D. K. (1982) Aqueous pyrite oxidation and the consequent formation of secondary iron minerals. In Acid Sulfate Weathering: Pedogeochemistry and relationship to manipulation of soil materials (eds. L. R. Hossaer, J. A. Kittrick, and D. F. Faming), Soil Science Society of American Press, Madison.
- Nordstrom D. K., Jenne E. A., and Ball J. W. (1979) Redox equilibria of iron in acid mine waters. ACS Symposium Series 93, 51-79.
- Rakcheyev A. D. and Chernyshev L. V. (1968) Energy of activation and chemical composition of pyrite as a function of its mode of synthesis. Dokl. Akad. Nauk. SSSR. 183, 1184-1187.
- Rimstidt J. D. (1980) The kinetics of silica-water reactions. Geochim. Cosmochim. Acta. 44, 1683-1699.
- Rising B. A. (1973) Phase relation among pyrite, marcasite and pyrrhotite below 300°C [Unpubl. PhD Thesis, Penn State Univ.].
- Shuey R. T. (1975) Semiconducting Ore Minerals. Elsevier, New York, 415 pp.
- Singer P. C. and Stumm W. (1969) Oxygenation of ferrous iron. FWQA Rep. 14010-0/69.
- Singer P. C. and Stumm W. (1970) Acid mine drainage: the rate determining step. Science 167, 1121-1123.
- Smith E. E., Svanks K., and Shumate K. S. (1968) Sulfide to sulfate reaction studies. In Second Symp. Coal Mine Drainage Res., 1-11. Pittsburgh.
- Smith F. G. (1940) Variation in the electrical conductivity of pyrite. Univ. of Toronto Stud., Geol. Sur., 44, 83-93.
- Smith F. G. (1942) Variation in the properties of pyrite. Amer. Min. 27, 1-19.

Stanton R. L. (1957) Studies of polished surfaces of pyrite and some implications. Can. Min. 6, 87-118.

Stokes H. N. (1901) On pyrite and marcasite. USGS Bull. 186.

Vaughan D. J. and Craig J. R. (1978) Mineral Chemistry of Metal Sulfides. Cambridge University Press, Cambridge, 493 pp.

Whittemore D. O. and Langmuir D. (1972) Standard electrode potential of $\text{Fe}^{3+} + \text{e}^{-} = \text{Fe}^{2+}$ from 5-35°C. Jour. Chem. and Engin. Data 17, 288-290.

APPENDIX I

CHARACTERIZATION OF RUN MATERIALS

Samples

The suitability of each sample for oxidation experiments was determined by reflected light optical microscopy and X-ray powder diffraction analyses. Purity of the sulfide mineral was the essential criterion for utility of a sample in the experiments. Many specimens originally collected for use in this project had to be eliminated due to contamination by minor inclusions of other sulfide minerals as determined by polished section examination or because the X-ray analysis showed a mixture of pyrite and marcasite. Samples were treated with 0.01M HCl as needed before runs to eliminate carbonate.

Polished section preparation

Polished sections were prepared for microscopic examination. A flat surface was cut on an approximately two centimeter diameter chip of each mineral sample. Cold-setting epoxy resin (Epofix resin mixed with Epofix hardener in an 8:1 ratio by weight) was used to cast the sample in a cylindrical polyethylene mold. Porous or fractured specimens were impregnated by placing the mold containing the specimen and mounting resin under vacuum for about 10 minutes. This procedure minimized plucking of material from the surface during polishing. Initial grinding was carried out on a grinding wheel of 240-micron diamond abrasive embedded in metal. Successive grinding steps included 300- and 600-micron fixed abrasives as described above. Rough polishing was begun

with 600-grit silicon carbide abrasive on a canvas covered lap for about 3 minutes, and completed using 15- and 6-micron diamond abrasives on a napless fabric for 5 minutes each. Final polishing was accomplished either by using a 1-micron diamond abrasive embedded in a napless cloth followed by 0.05-micron γ -Al₂O₃ suspended in water on microcloth or by at least 24 hours in a Syntron vibropolishing machine. The sections were thoroughly washed and cleaned between steps using an ultrasonic cleaner to prevent contamination by carry over of abrasive from one step to the next. Most of the finished polished sections were partially etched with nitric acid after a preliminary examination. Half of the polished surface was covered with melted paraffin and then exposed to the acid fumes. This process of microchemical etching brings out inner- and intra-grain textures that are not normally visible petrographically in a polished section of an isotropic mineral. Polished sections were stored in a desiccator.

X-ray diffraction

Randomly oriented powder mounts were prepared by grinding a small portion of the sample in an acetone slurry using an agate mortar and then dispersing the slurry on a glass petrographic slide. Powder x-ray diffraction patterns were measured using a Norelco automated diffractometer employing a monochromator set for nickel-filtered CuK_α radiation. One oscillation from 20° to 50° in 2θ was scanned at 2° per minute for each sample. In this 2θ interval three of the pyrite and marcasite peaks coincide, but there are two unique pyrite reflections and three unique marcasite reflections of sufficient intensity to

distinguish between the two polymorphs (see Table 5). These are the {111} and {211} reflections for pyrite and for marcasite the {110}, {120} and {210} reflections. Any sample determined to be a pyrite/marcasite mixture was eliminated as possible experimental run material.

Hand sample and Petrographic descriptions of run samples

PY-01: This specimen is a 10 inch diameter saucer-shaped concretion which originated in a coal underclay. It was collected in Kentucky from beds associated with fairly high rank coals of the Pennsylvania coal measures. Diagenetic temperatures likely reached 65 to 100°C (Rimstidt, pers. comm., 1981). It is an aggregate of cryptocrystalline framboidal pyrite crystals with subhedral microcrystalline pyrite grains lining tiny vugs and elongate burrow-shaped areas. The framboidal texture is evident only in the etched portion of the section, where vigorous reaction at the grain boundaries highlighted the texture. The larger pyrite grains in the vugs and burrows were more acid resistant than the framboidal material. The framboidal texture is predominant, and at very high magnification (50x) euhedral crystal faces and the tiny inter-grain voids characteristic of framboidal aggregates can be seen. Except for microscopic cracks and voids and traces of organic matter, this concretion is essentially a homogeneous mass of pyrite. No distinct anisotropy was observed. X-ray powder patterns indicate that this is a pure pyrite.

PY-02: This is a small concretion collected from a dolomitized Silurian carbonate at the Napoleon Quarry in Southern Indiana. It was probably

TABLE 52 θ CALCULATIONS FOR POWDER X-RAY DIFFRACTION PATTERNS

<u>PYRITE</u>			<u>MARCASITE</u>		
I/I ₁	d(A)	2 θ	I/I ₁	d(A)	2 θ
35	3.128	28.54	40	3.44	25.9
85	2.709	33.07	100	2.71	33.1
65	2.423	37.11	25	2.41	37.3
50	2.2118	40.80	25	2.32	38.8
40	1.9155	47.47	2	2.05	44.2
			30	1.91	47.6

Comments

I/I₁ and d(A) values are from ASTM cards 6-0710 pyrite and 3-0799 marcasite.

2 θ calculated from $2\theta = 2\sin^{-1}[\frac{1}{2}\lambda(1/d^2)^{\frac{1}{2}}]$

$\lambda = 1.542$, CuK $_{\alpha}$ radiation.

Standard conditions: CuK $_{\alpha}$ radiation
 40 keV, 20 ma
 Time Constant = 1
 100 or 200 counts per second
 2° per minute, 20° to 50° 2 θ

Pyrite and marcasite distinguished in the 2 θ range 20° to 50° by unique reflection for pyrite at 40.80° and 28.54°; for marcasite at 25.9°, 38.8°, and where sufficiently strong, 44.2°.

formed in a carbonate mud less than two meters deep at temperatures much less than 50°C (Rimstidt, pers. comm., 1981). It consists entirely of subhedral to euhedral cubic pyrite crystals intergrown with some traces of carbonate and organic material. Large voids are outlined by the cubic crystal faces. The pyrite crystals are compactly intergrown near the center of the concretion, becoming less compact and less euhedral toward the exterior of the concretion. At high magnification the pyrite is seen to contain a multitude of minute fractures and pits. Etching brought out growth zoning not visible in the unetched crystals. At high magnification these growth lines appear as 'phantom' crystal faces outlined by inclusions of some other material (fluid inclusions?) which adhered to the cube surfaces during a lull in deposition.

PY-05: This is an FeS₂ concretion in the shape of a 'sand dollar' in which form it is typically thought to be marcasite. However, X-ray powder patterns show that this is pyrite; no marcasite peaks were observed. A number of these 'sand dollars' were collected from a medium to high rank volatile coal in Illinois. Temperatures of formation were likely below 100°C (Rimstidt, pers. comm., 1981) Both a horizontal and vertical cross-section of one of the dollars were cut and polished. The vertical section shows a suture zone along the center of its length along which the elongate sulfide mineral grains nucleated and grew. These grains fan out and impinge upon each other toward the top and the bottom of the dollar, forming a homogeneous mass of FeS₂. A distinct anisotropy on the length of these fan-and-spindle shaped grains

was enhanced by etching. A similar effect was observed in the horizontal cross-section of these grains. Some of the elongate grains reacted more vigorously with the acid. At higher magnifications, the etching revealed a host of microscopic cracks and voids within each grain. This spongy texture is typical of dry inversion accompanied by a decrease in volume, in this case, from marcasite to pyrite. A distorted pyrite structure resulting from the marcasite to pyrite inversion may account for the anisotropic effects.

PY-04: Large homogeneous compact masses of polycrystalline pyrite were collected from petroleum filled vugs in dolomitized limestone at the Renseleer Quarry in Indiana. The vug filling sulfide was deposited from Mississippi Valley Type oil field brines at temperatures of 100 to 150°C (Rimstidt, pers. comm., 1981). This pyrite was chosen as standard test run material because of its homogeneity and the large quantity obtained. Open space deposition is evidenced by euhedral faces around the exterior of the masses, which grade into massive pyrite toward the centers. The pyrite is non-descript in unetched polished form, grain boundaries being visible only as tiny fracture-like lines. A weak anisotropism can be seen in the individual grains at high illumination. Half of the section was etched, the chemical reaction enhancing the interior grain boundaries and hair-like fractures within grains. Differential reaction of the grains in the mass to the etchant is likely due to crystallographic direction with (100) and (210) being the most resistant, i.e., turning less brown. The anisotropy was severely enhanced by the etchant, but this is probably a property of the oxide

reaction product formed which renders the attacked surface brown.

PY-06: This pyrite was collected from the Bear Hole Mine in the Upper Mississippi Valley lead-zinc district near Schullsburg, Wisconsin. Fluid inclusion studies indicate formation temperatures of 100 to 160°C (Rimstidt, pers. comm., 1981). This sample consists of pure polycrystalline aggregates of pyrite, which are highly fractured between and within grains. The only anisotropy shown by the pyrite is a polishing hardness effect visible as oriented 'lamellae' of pyrite within the larger grains. These can be seen as shallow pits or raised areas which under doubly polarized light impart a slight anisotropic effect, probably due to shadows. The appearance of the hand specimen is of a compact aggregate of crowded and distorted pyrite crystals showing a number of crystal morphologies and pervasive growth striations. The tiny 'lamellae' are parallel to the major fractures in their host crystal. Upon etching, these 'lamellae' were much more resistant to the acid attack than the surrounding pyrite grain. Some sort of growth stress may be responsible for the distorted appearance of the crystals, the fracturing, and the consistent orientation of these harder 'lamellae' by twinning. The 'lamellae' may represent a different crystallographic direction, more resistant to the acid, e.g., (100) or (210). The etching also brought out numerous tiny cleavages and fractures not originally visible in the large pyrite crystals.

PY-10: These are cubes of pyrite in a schist from Pennsylvania obtained from Ward's. The cubes are fractured and some contain small inclusions of quartz. In polished section, the pyrite is distinctly

anisotropic, with intersections of growth zones visible at the cube corners. These growth zones may contain significant amounts of nickel or cobalt. Only the cleanest cubes (no silicates) were selected as run material.

PY-11: This is a mass of very fine fibrous pyrite grains radiating from a central point and fanning outward to form an almost botryoidal exterior shape. This specimen, obtained from the Mineralogical Research Company, San Jose, California, was labeled as marcasite from Pas-de-Calais, Northern France. However, X-ray powder patterns show only pyrite peaks. The feathery appearance of the terminations of the fine fibrous crystals on the tarnished exterior of the globular mass do resemble marcasite cockscombs, but the interior is bright and brassy yellow. In polished section the individual radial fibrous pyrite crystals contain multitudes of cracks and show distinct anisotropy in the lengthwise section. There are large voids at the grain boundaries. The spongy texture is characteristic of the marcasite to pyrite inversion.

MC-01: This is a vug filling encrustation of cockscomb marcasite over sphalerite and calcite collected from the Bear Hole Mine in the Upper Mississippi Valley lead-zinc district near Shullsburg, Wisconsin. Fluid inclusion studies indicate formation temperatures of 100 to 160°C (Rimstidt, pers. comm., 1981). There are fine intergrowths of pyrite and marcasite adjacent to the calcite gangue. Microscopic voids at pyrite-marcasite and pyrite-pyrite grain contacts appear at high magnification, but the pyrite itself shows no anisotropy and does not

exhibit the characteristic spongy texture of inversion from marcasite. Pyrite disappears abruptly as fine marcasite grades into coarse marcasite toward the exterior of the encrustation. In doubly polarized light the marcasite exhibits coarse lamellar twinning in crystals that radiate upward and outward. In linearly polarized light the differences in polishing hardness between different crystallographic directions in the polycrystalline marcasite aggregate are striking. The pyrite and marcasite may have been deposited simultaneously during pulsating periods of deposition without equilibrium. The pure marcasite exterior was separated for run material.

MC-02: This is a vug filling polycrystalline growth of marcasite collected from the dolomitized limestone at the Renseleer Quarry in Indiana. The sulfides were deposited from Mississippi Valley type oil field brines at temperatures of 100 to 150°C. The marcasite has grown radially from a dolomite and pyrite substrate. The dolomite gangue contains tiny rounded to ragged and angular anhedral pyrite grains ranging widely in size. Larger masses of pyrite adjacent to the dolomite and the marcasite contain tiny marcasite crystals and have discontinuous rims of marcasite. The pyrite shows a very weak anisotropism and is very porous, with microscopic voids and linear cracks. The marcasite shows a brilliant radial growth structure in fine crystals from the dolomite/pyrite surfaces, grading into very coarse crystals with coarse lamellar growth twins toward the exterior of the aggregate. The pure marcasite exterior was separated for run material.

MC-03: This specimen was obtained from the Mineralogical Research

Company of San Jose, California. It is from the Dana locale near Joplin in Jasper County, Missouri. Cockscomb marcasite crystals encrust a large (40mm) galena cube. Rhombohedral calcite crystals are sparsely intergrown with the marcasite. Marcasite becomes intergrown with galena near the edge of the large cube. In polished section the marcasite crystals are homogeneous. Care was taken to separate any galena from the marcasite before preparation for run material.

APPENDIX II

EXPERIMENTAL DESIGN AND PROCEDURES

APPARATUS:

Water bath: Experiments were performed in a constant temperature water bath employing a mercury relay temperature control which could maintain temperatures to $\pm 0.3^{\circ}\text{C}$ up to 50°C . Cold tap water was circulated through cooling coils in the water bath to maintain 25°C temperatures. A custom-fit cover for the water bath/reaction vessel (500 ml Kimax reaction kettle) assembly was machined out of transparent Plexiglass with access ports for electrode and stirring impeller.

Stirring assembly: A Richards stirring motor with solid state variable speed control was equipped with a glass impeller. This portable stirring assembly was suspended over the water bath by a metal arm clamped to a heavy-duty laboratory stand. The impeller was placed in the run solution before the beginning of each run by manually lowering it through an access port in the water bath cover. Standard stirring speed was set at 700 rpm (stirring rate = 4 on variable speed control unit).

Computer automation of potential measurements: A Fisher combination platinum/saturated KCl/Ag-AgCl electrode was used to measure the redox potential of the run solutions. An Apple II Plus microcomputer with Disk II Operating System monitored each run via an Interactive Microware Adalab interface card utilizing a program adapting copyrighted Interactive Microware subroutines. The program, EHREAD,

reads the electrode current and converts it to a potential in millivolts. One hundred readings were taken during the course of each 250 minute run in 2.5 minute intervals and simultaneously recorded on an Epson MX-80 printer.

PROCEDURES:

Standard 0.001 molal (56 ppm) ferric chloride run solution: The run solution was prepared by combining 0.25 ml of 75% $\text{FeCl}_3 \cdot 6\text{H}_2\text{O}$ Fisher Chemical Reagent with 1 liter distilled/deionized H_2O previously acidified to pH 2 with 1.5 ml concentrated HCl. Five hundred milliliters of this solution was then transferred to the reaction vessel and brought to run temperature in the water bath with the electrode immersed.

Preparation of run material: The sulfide run material was freshly prepared for each run by comminution in a Tekmar Model A10 Analytical Mill and then sized using 50 mm diameter brass laboratory sieves to isolate the 100 to 200 mesh size fraction. A magnet was passed over this isolated fraction to remove any iron filings derived from the metal grinding chamber or blade of the micromill. A 1.0000 ± 0.0005 gram sample of this freshly prepared sulfide material was used in each run. Run material was added to the solution after 4 readings of the run solution potential (already brought to run temperature) were recorded (about 10 minutes).

pH measurements: Solution pH was checked before and after each run using an Orion Research Microprocessor pH/millivolt meter Model 811 with an Orion Research pH electrode. The final pH of the run solution

was always within 0.04 pH units of the initial pH of 2.00.

Sample analysis: The concentrations of ferrous and of total iron in the initial and final run solution of each experiment were determined spectrophotometrically by the assay procedure described below. In order to assay the solution for iron during a run, a 5 ml volume aliquot was extracted at selected intervals during several experiments. These samples were extracted through the impeller port using a syringe and then discharged through a 0.8 micron Millex-PF Millipore filter before removing an aliquot for the iron assay.

Iron Assay: A method for simultaneous spectrophotometric determination of ferrous and total iron was adapted from the procedure of Harvey, et al. (1955). This method is based on the difference in absorption spectra of the reddish-orange ferrous-phenanthroline complex and the yellow ferric-phenanthroline complex. Absorption curves at three different concentrations for both the ferrous- and ferric-phenanthroline complexes were determined to check the wavelength of intersection against that determined by Harvey, et al. These absorption curves show the two complexes to have identical absorbance coefficients at 393 nm rather than at 396 nm, as determined in the original study. The absorbance for total iron in our experimental solutions was therefore measured at the shorter wavelength. This difference in the wavelength of intersection between the two studies may be caused by differences in the ambient laboratory temperature, cuvette construction, or purity of water used to mix reagents.

Standard concentration curves at 512 nm were prepared for both

the ferrous and the ferric complexes. Because the absorbances of the two complexes at 393 nm are additive, Harvey, et al. state that the standard curve for total iron at 393 nm may be obtained from the solutions of either complex. However, for this study, absorbance measurements were made on solutions of both complexes at 393 nm and compared before constructing the total iron concentration curve. These measurements at 393 nm for the two complexes duplicated within 1.3% on the average, with a maximum deviation of 5.6%. The average precision of the 1,10-phenanthroline method is 1.5% for total iron and 2.3% for ferrous iron (Harvey, et al., 1955).

Instruments: A Bausch & Lomb Spectronic 21 spectrophotometer, Model MV, with 10 mm pathlength cuvettes, was used for the spectrophotometric measurements.

Preparation of reagent solutions: Use distilled/deionized H₂O for all dilutions.

1,10-Phenanthroline (1%): With stirring, dissolve 1.00 gram reagent grade 1,10-phenanthroline monohydrochloride monohydrate in water in a 100 ml volumetric flask. Dilute to final volume, transfer to a 2 ml fixed volume automatic pipette dispenser, and store in the dark.

Potassium biphthalate buffer (0.2 M, pH = 3.98): With stirring, dissolve 10.21 gram of reagent grade potassium acid phthalate in water in a 250 ml volumetric flask. Dilute to final volume and transfer to a 5 ml fixed volume automatic pipette dispenser.

Procedure:

1. Add a sample to a 25 ml volumetric flask to give between 0 and 10

mg of iron.

2. Add 2 ml phenanthroline reagent and swirl for 30 seconds.
3. Add 5 ml buffer and swirl.
4. Dilute to mark and mix.
5. Read absorbance at 512 nm and 393 nm immediately and not later than 30 minutes after complexes are formed.

Calculation of results:

1. Determine the concentration of total iron and the approximate concentration of ferrous iron from standard curves at 393 and 512 nm, respectively.
2. Obtain the approximate concentration of ferric iron by difference.
3. From the standard curve for ferric at 512 nm find the absorbance value corresponding to the approximate ferric concentration.
4. Subtract this absorbance value ($A(512)$ for ferric) from the observed absorbance at 512 nm to obtain the absorbance at 512 nm due to ferrous iron. Obtain the corrected concentration of ferrous from its curve at 512 nm.
5. For the correct concentration of ferric, subtract the corrected ferrous concentration from the total iron concentration already determined.

APPENDIX III
COMPUTER PROGRAMS

IRON - A PROGRAM TO CALCULATE THE DISTRIBUTION
OF IRON SPECIES IN ACID CHLORIDE SOLUTIONS

IRON is a FORTRAN program which calculates the distribution of iron species in a chloride/sulfate solution at 25°Celsius. It was designed to help interpret experimental data on the oxidation rate of pyrite in an acid, ferric-chloride medium. IRON consists of a main program IRONA, and a series of subroutines, ISTR, GAMMA, and DISTN.

Input format is 3F10.0 and is submitted in the following order: MCL = total chloride concentration, TOTFE = total iron concentration, and TOTFE3 = total ferric concentration (all in molal concentration units). An example of input format can be found at the end of the IRON program listing in this appendix. The main program, IRONA, reads the input data, calculates the ferrous iron concentration by difference ($TOTFE2 = TOTFE - TOTFE3$), calculates the total sulfate concentration according to the stoichiometry of the pyrite oxidation reaction ($MSO4 = TOTFE2 / 7.0$), varies the pH from 0.2 to 3.4 in increments of 0.2, and calls into action the subroutine series for each pH value.

The species concentration values calculated by the subroutine series are then recast by IRONA into log of concentration and percent of total ferrous or ferric. Eh is calculated from the ferric-ferrous activity ratio using the Nernst relation. The output format handled by

IRONA lists pH, ionic strength, total iron and total ferrous, ferric, sulfate, and chloride values. Columns showing percent of total ferrous or ferric iron, log concentration and individual ionic activity coefficient values for each species are also printed for each pH. This output format facilitates plotting of the data on speciation diagrams. The number of iterations required in calculating the distribution of iron species at each pH is also listed at the bottom of each page of output, along with the calculated ferric/ferrous activity ratio and Eh. A program listing of IRON is included in this appendix. One page of output produced by IRON is shown as an example in Figure 4. Figure 5 shows one of the speciation diagrams constructed from IRON output.

The subroutines called by IRONA are described separately below, in order of their implementation.

ISTR: The main function of this subroutine is to calculate the stoichiometric ionic strength of the solution. An iterative method to determine the true ionic strength is not necessary here because use of the extended form of the Debye-Huckel expression later in the program will account for the short-range, ion-pairing effects.

- 1) Assuming that concentration is approximately equal to activity for H^+ and OH^- , the concentrations of hydrogen ion and of hydroxyl ion are calculated from the definition of pH.
- 2) Since the experimental solutions are based in a chloride medium (ferric chloride in 0.01M HCl), there will be a chloride excess. Therefore, the input chloride concentration value can be adjusted to balance the total positive and negative charges in the solution.

Assuming complete dissociation of the major ionic species, the total positive charge $CHGX = 2M(Fe2) + 3M(Fe3) + M(H)$ and the total negative charge $CHGY = M(Cl) + 2M(SO4) + M(OH)$ are calculated. The chloride concentration is then adjusted to account for any difference in these sums, thus providing an electrically neutral solution.

- 3) The new chloride concentration, the hydrogen and hydroxyl ion concentrations, and the input concentration data for ferrous, ferric, and sulfate are used to calculate the stoichiometric ionic strength.

GAMMA: This subroutine calculates the individual ionic activity coefficient, γ_i , for each unassociated ion (i) and for each possible ion pair (i). The extended form of the Debye-Huckel expression used here:

$$\log \gamma_i = -Az_i^2\sqrt{I} / (1 + Ba_i\sqrt{I})$$

takes into account the long-range electrostatic forces (the numerator on the right) and the modification of these coulombic forces by the short-range interactions (the denominator on the right) (Robinson & Stokes, 1955, p.231). A and B are parameters related to the dielectric constant of the solvent water (which is a function of temperature) and are given as constants at 25°C (Stumm & Morgan, 1981). I is the ionic strength, the value of which is supplied by the subroutine ISTR and z_i is the charge on the ion or ion pair. The a_i value in the denominator is the

closest approach parameter (CAP). The CAP's of the free dissociated ions were assigned their established values (Kielland, 1936 and Garrels & Christ, 1965). CAP values for the majority of the charged ion pairs, however, are not readily available in the literature. Therefore, values were taken from Truesdell and Jones (1974) or estimations were made by comparison with the published values. Activity coefficients for non-charged ion pairs were assigned a value of 1.0 (Millero and Schreiber, in press).

DISTN: Subroutine DISTN calculates the distribution of free and associated species in the solution.

- 1) The activities of the hydroxyl and hydrogen ion are calculated according to the definition of pH.
- 2) The distribution of sulfate among SO_4^{2-} and HSO_4^- is calculated analytically from the total sulfate value. Combining the sulfate mass balance equation with the bisulfate association constant expression gives:

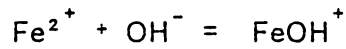
$$m_{\text{HSO}_4^-} = \frac{(K_{\text{assoc}})(a_{\text{H}^+})(\gamma_{\text{SO}_4^{2-}})(\text{tot}m_{\text{SO}_4^{2-}})}{\{\gamma_{\text{HSO}_4^-} + (K_{\text{assoc}})(a_{\text{H}^+})(\gamma_{\text{SO}_4^{2-}})\}}.$$

Substituting this bisulfate concentration back into the mass balance equation results in a value for the sulfate concentration.

- 3) Activities of the free ionic species are calculated from $a = \gamma m / \gamma^\circ m^\circ$ where $\gamma^\circ = 1$ and $m^\circ = 1$ for the hypothetical ideal one molal standard state. The concentrations for ferrous and ferric are as

given in the input data (i.e. equal to total ferrous and total ferric, respectively), hydrogen and hydroxyl ion concentrations as given by pH. The adjusted concentration values for chloride ion (from the charge balancing in ISTR) and sulfate (from the sulfate-bisulfate distribution computation) are used here.

- 4) A continuous fraction iteration method is used to calculate the concentrations of the ferric ion pairs. The iteration begins by guessing that the original input value TOTFE3 actually represents the free unassociated ferric ion concentration. The activity of ferric calculated in 3) from this value is then used to calculate the concentrations of each of the ion pairs. The derivation for the general form of these equations is given in an example below:



$$K_{\text{assoc}} = a_{\text{FeOH}^+} / a_{\text{Fe}^{2+}} a_{\text{OH}^-}$$

$$K_{\text{assoc}} = m_{\text{FeOH}^+} \gamma_{\text{FeOH}^+} / a_{\text{Fe}^{2+}} a_{\text{OH}^-}$$

$$m_{\text{FeOH}^+} = K_{\text{assoc}} a_{\text{Fe}^{2+}} a_{\text{OH}^-} / \gamma_{\text{FeOH}^+}$$

K_{assoc} is a constant at 25°C (see Table 5 and Appendix III references for sources of data). Cation and anion activities are from 1) and 3) above. γ_{FeOH^+} is from subroutine GAMMA.

- 5) After the concentrations of all the ferric species are calculated, the sum of the concentrations of all these species is determined (SUMFE3) and this value is tested against the original input value

TOTFE3. If these values differ by greater than 0.01%, the present concentration of free ferric is multiplied by the ratio of true total ferric (TOTFE3) to calculated total ferric (SUMFE3), a new activity of Fe^{3+} is calculated, and the concentration calculations are repeated. The iteration is complete if the values of SUMFE3 and TOTFE3 differ by 0.01% or less.

- 6) An iteration for the ferrous species exactly analogous to that for the ferric species is then performed. Only one or two iterations are normally required for the ferrous calculations, whereas two to five iterations are required for ferric. When the iterations are complete, control is returned to the main program.

LIST OF VARIABLE NAMES USED IN PROGRAMS IRON AND REDOX

AA = MOLAL DEBYE HUCKEL COEFFICIENT A
 AX = ACTIVITY OF CATION GIVEN AS X
 AY = ACTIVITY OF ANION GIVEN AS Y
 AXY = ACTIVITY OF THE ION PAIR GIVEN AS XY
 BB = MOLAL DEBYE HUCKEL COEFFICIENT B
 CAP = CLOSEST APPROACH PARAMETER
 CHG = CHARGE ON THE IONIC SPECIES GIVEN AS X, Y, OR XY
 CL = DESIGNATION FOR CHLORIDE ION
 EH = EH OF THE SOLUTION IN VOLTS
 EMF = MEASURED SOLUTION POTENTIAL IN VOLTS
 FE2 = DESIGNATION FOR FERROUS IRON
 FE3 = DESIGNATION FOR FERRIC IRON
 GM = INDIVIDUAL IONIC ACTIVITY COEFFICIENT (FOR X, Y, XY)
 H = DESIGNATION FOR HYDROGEN ION
 IST = STOICHIOMETRIC IONIC STRENGTH
 ITFE2 = NUMBER OF ITERATIONS REQUIRED FOR FERROUS
 ITFE3 = NUMBER OF ITERATIONS REQUIRED FOR FERRIC
 LOGX = LOG OF CONCENTRATION OF CATION
 LOGY = LOG OF CONCENTRATION OF ANION
 LOGXY = LOG OF CONCENTRATION OF ION PAIR XY
 MCL = MOLAL CONCENTRATION OF CHLORIDE ION
 M2EH = FREE FERROUS CONCENTRATION CALCULATED FROM EH
 M3EH = FREE FERRIC CONCENTRATION CALCULATED FROM EH
 MFE2 = MOLAL CONCENTRATION OF FERROUS ION
 MFE3 = MOLAL CONCENTRATION OF FERRIC ION
 MSO4 = MOLAL CONCENTRATION OF SULFATE ION
 MX = MOLAL CONCENTRATION OF CATION
 MY = MOLAL CONCENTRATION OF ANION
 MXY = MOLAL CONCENTRATION OF THE ION PAIR
 OH = DESIGNATION FOR HYDROXYL ION
 PH = NEGATIVE LOG OF THE ACTIVITY OF HYDROGEN ION
 PRCT = PERCENT OF TOTAL FERROUS OR FERRIC IRON
 RAT = FERRIC/FERROUS ACTIVITY RATIO
 SO4 = DESIGNATION FOR SULFATE ION
 SUMFE2 = CALC'D SUM OF CONCENTRATIONS OF FERROUS SPECIES
 SUMFE3 = CALC'D SUM OF CONCENTRATIONS OF FERRIC SPECIES
 SUMXY2 = CALC'D SUM OF CONCENTRATIONS OF FERROUS ION PAIRS
 SUMXY3 = CALC'D SUM OF CONCENTRATIONS OF FERRIC ION PAIRS
 TAC = TOTAL STOICHIOMETRIC ACTIVITY COEFFICIENT RATIO
 TOTFE = TOTAL CONCENTRATION OF IRON
 TOTFE2 = TOTAL CONCENTRATION OF FERROUS IN ALL SPECIES
 TOTFE3 = TOTAL CONCENTRATION OF FERRIC IN ALL SPECIES
 X = DESIGNATION FOR CATION
 Y = DESIGNATION FOR ANION
 XY = DESIGNATION FOR ION PAIR
 ZX = CHARGE ON THE CATION
 ZY = CHARGE ON THE ANION
 ZXY = CHARGE ON THE ION PAIR

TABLE 6
DISTN SPECIES LIST

SPECIES#	SPECIES	SYMBOL	LOG K(assoc) [■]	REF [■]	CAP [•]
1	H ₂ O	H2O	14		
2	HSO ₄ ⁻	HSO4	1.99	2,3	4.5
3	H ₂ SO ₄	H2SO4	-3.00	5	
4	HCl	HCL	-3.00	5	
-FERROUS-					
5	FeOH ⁺	FE2OH	4.5	1,2	5.0
6	Fe(OH) ₂ (aq)	FE2OH2	7.4	1,2	
7	Fe(OH) ₃ ⁻	FE2OH3	11.0	1	5.5
8	FeSO ₄ (aq)	FE2SO4	2.2	2	
9	FeHSO ₄ ⁺	FE2HSO	1.1	(est'd)	5.4
-FERRIC-					
10	FeOH ⁺²	FEOH	11.81	1,2	5.0
11	Fe(OH) ₂ ⁺	FEOH2	22.33	1,2	5.0
12	Fe(OH) ₃ (aq)	FEOH3	30.0	1	
13	Fe(OH) ₄ ⁻	FEOH4	34.4	1,2	5.4
14	FeSO ₄ ⁺	FESO4	4.04	2	5.0
15	Fe(SO ₄) ₂ ⁻	FESO42	5.40	2	5.5
16	FeHSO ₄ ⁺²	FEHSO4	0.6	4	6.0
17	FeCl ⁺²	FECL	1.48	2	5.0
18	FeCl ₂ ⁺	FECL2	2.13	2	5.0
19	FeCl ₃ (aq)	FECL3	-0.7	2	
20	Fe ₂ (OH) ₂ ⁺⁴	DFEOH2	25.05	1,2	11.0
21	Fe ₃ (OH) ₄ ⁺⁵	TFEOH4	49.7	1,2	11.0
-FREE CATIONS-					
1	H ⁺	H	-	-	9.0
2	Fe ⁺²	FE2	-	-	6.0
3	Fe ⁺³	FE3	-	-	9.0
-FREE ANIONS-					
1	OH ⁻	OH	-	-	3.5
2	SO ₄ ⁻²	SO4	-	-	5.0
3	Cl ⁻	CL	-	-	3.5

■ Notes on LOG K(assoc) values:

- SPECIES# 5) LOG K = 4.41 @ I = 0.002 from Davison (1979)
 SPECIES# 7) LOG K = 10.0 @ I = 0.0 from Smith & Martell (1976)
 SPECIES# 8) LOG K = 1.95 @ I = 0.002 from Davison (1979)
 SPECIES#19) LOG K = -0.7 @ I = 1.0 from Smith & Martell (1976)

■ LOG K(assoc) references, see next page.

• Truesdell & Jones (1974) or estimated as described in text.

APPENDIX III REFERENCES

1. Baes C.F. Jr. and Mesmer R.E. (1976) The Hydrolysis of Cations, Wiley-Interscience, New York, pp 226-237.
2. Smith, R.M. and A.E. Martell (1976) Critical Stability Constants Vol. 4. Inorganic Complexes, Plenum Press, New York, 257 pp.
3. Young, T.F., C.R. Singleterry, and I.M. Klotz (1978) Ionization constants and heats of ionization of the bisulfate ion from 5 to 55°C, J. Phys. Chem. 82, 671-674.
4. Sapieszko, R.S., R.C. Patel, and E. Matijevic (1977) Ferric hydrous sols 2. Thermodynamics of aqueous hydroxo and sulfato ferric complexes, J. Phys. Chem. 81, 1061-1068.
5. Stumm, W. and J.J. Morgan (1981) Aquatic Chemistry, 2nd Edition, Wiley-Interscience, New York, 780 pp.
6. Davison, W. (1979) Soluble inorganic ferrous complexes in natural waters, Geochim. et Cosmochim. Acta 43, 1693-1696.
7. Garrels, R.M. and C.L. Christ (1965) Solutions, Minerals, and Equilibria, Freeman, Cooper & Company, San Fransisco, 450 pp.
8. Truesdell, A.H. and B.F. Jones (1974) WATEQ, A computer program for calculating chemical equilibria of natural waters, USGS J. Res. 2, 233-248.
9. Robinson, R.A. and R.H. Stokes (1955) Electrolyte Solutions, Academic Press, Inc., New York, 559pp.
10. Kielland J. (1937) Individual activity coefficients of ions in aqueous solutions, J. Amer. Chem. Soc. 59, 1675-1678.
11. Millero F.J. and Schreiber D.R. (in press) Use of the ion pairing model to estimate activity coefficients of the ionic components of natural waters. Amer. J. Sci.

IRON PROGRAM LISTING

```

C$JOB          RIMSTIDT
C$OPTIONS PAGES=40
C$OPTIONS NOLIST
C *****
C * PROGRAM IRONA::3-1-82::C.L. WIERSMA *
C * A PROGRAM TO CALCULATE THE DISTRIBUTION OF IRON SPECIES IN A *
C * SOLUTION WITH CHLORIDE AND SULFATE AT 25 DEGREES CELSIUS. *
C *****
C
  REAL MX, MY, MXY, PH, EH, CHGX, CHGY, IST, GMX, GMY, GMXY, CAPX,
  $CAPY, CAPXY, AX, AY, AXY, TOTFE3, TOTFE2, SUMXY3, SUMXY2, SUMFE3,
  $SUMFE2, LOGXY, LOGX, LOGY, R, PRCT, MSO4, MCL, TOTFE, RAT
  INTEGER H, FE2, FE3, OH, SO4, CL, X, Y, XY, ZX, ZY, ZXY, H2O,
  $HSO4, H2SO4, HCL, FE2OH, FE2OH2, FE2OH3, FE2SO4, FE2HSO, FEOH,
  $FEOH2, FEOH3, FEOH4, FESO4, FESO42, FEHSO4, FECL, FECL2, FECL3,
  $DFEOH2, TFEOH4, ITFE2, ITFE3
  DIMENSION ZX(3), ZY(3), ZXY(21), MX(3), MY(3), MXY(21), CAPX(3),
  $CAPY(3), GMX(3), GMY(3), GMXY(21), AX(3), AY(3), AXY(21),
  $LOGXY(21), LOGX(3), LOGY(3), PRCT(21)
  DATA H, FE2, FE3/1, 2, 3/
  DATA OH, SO4, CL/1, 2, 3/
  DATA H2O, HSO4, H2SO4, HCL, FE2OH, FE2OH2, FE2OH3, FE2SO4,
  $FE2HSO, FEOH, FEOH2, FEOH3, FEOH4, FESO4, FESO42, FEHSO4, FECL,
  $FECL2, FECL3, DFEOH2, TFEOH4/1, 2, 3, 4, 5, 6, 7, 8, 9, 10, 11,
  $12, 13, 14, 15, 16, 17, 18, 19, 20, 21/
  DATA (ZX(I), I=1,3)/1, 2, 3/
  DATA (ZY(J), J=1,3)/-1, -2, -1/
  DATA (ZXY(L), L=1,21)/0, -1, 0, 0, 1, 0, -1, 0, 1, 2, 1, 0, -1,
  $1, -1, 2, 2, 1, 0, 4, 5/
  DATA (CAPX(X), X=1,3)/9.0, 6.0, 9.0/
  DATA (CAPY(Y), Y=1,3)/3.5, 5.0, 3.5/
C
C*****INPUT-READ CONC'NS OF IONS
  READ (5,10) MCL, TOTFE, TOTFE3
  10 FORMAT (3F10.0)
C
C*****CALCULATE FE2 AND SO4 CONC'NS
  TOTFE2=TOTFE-TOTFE3
  MSO4=TOTFE2/7.0
C
C*****STEP UP PH IN INCREMENTS OF 0.2 FROM PH=0.2 TO PH=3.4
  DO 20 I=2,34,2
  R=I
  PH=R/10.0
  MX(FE2)=TOTFE2
  MX(FE3)=TOTFE3
  MY(SO4)=MSO4
  MY(CL)=MCL
  15 CALL ISTR(IST, PH, MX, MY, MXY, GMX, GMY, GMXY)
  CALL GAMMA(IST, PH, MX, MY, MXY, GMX, GMY, GMXY)
  CALL DISTN(IST, PH, MX, MY, MXY, GMX, GMY, GMXY, TOTFE3, TOTFE2,

```

```

      $SUMFE2, SUMFE3, ITFE2, ITFE3, AX)
C
C*****CALCULATE WHAT PERCENT OF THE TOTAL IRON EACH SPECIES
C REPRESENTS.
      PRCT(FE3)=(MX(FE3)/TOTFE3)*100.0
      DO 25 M=10,21
25  PRCT(M)=(MXY(M)/TOTFE3)*100.0
      PRCT(FE2)=(MX(FE2)/TOTFE2)*100.0
      DO 26 N=5,9
26  PRCT(N)=(MXY(N)/TOTFE2)*100.0
C
C*****CALCULATE EH FROM ACTIVITY RATIO
      RAT=(PRCT(FE3)*AX(FE3))/(PRCT(FE2)*AX(FE2))
      EH=(0.771)+(0.02569)*ALOG(RAT)
C
C*****TAKE THE LOG OF THE CONCENTRATION VALUES TO FACILITATE DATA
C PLOTTING OUTPUT.
      DO 30 J=2,21
      LOGXY(J)=ALOG10(MXY(J))
30  CONTINUE
      DO 40 K=1,3
      LOGX(K)=ALOG10(MX(K))
40  CONTINUE
      DO 50 L=1,3
      LOGY(L)=ALOG10(MY(L))
50  CONTINUE
C
C*****PRINT OUTPUT WHEN ITERATION IS COMPLETED.
      WRITE (6,60) PH, IST, TOTFE2, TOTFE3, MSO4
60  FORMAT (1H1, 10X, 'PH=', F4.2, 6X, 'IST=', F7.4, 6X, 'TOTFE2=',
      $F8.6, 6X, 'TOTFE3=', F8.6, 6X, 'MSO4=', F8.6)
      WRITE (6,65) TOTFE, SUMFE2, SUMFE3, MCL
65  FORMAT (22X, 'TOTFE=', F8.6, 5X, 'SUMFE2=', F8.6, 6X, 'SUMFE3=',
      $F8.6, 6X, 'MCL= ', F8.6, ///)
      WRITE (6,70)
70  FORMAT (10X, 'SPECIES', 4X, 'PRCT', 4X, 'LOGC', 4X, 'GAMMA', 6X,
      $'SPECIES', 4X, 'PRCT', 4X, 'LOGC', 4X, 'GAMMA')
      WRITE (6,75)
75  FORMAT (10X, 'FERROUS', 31X, 'FERRIC', //)
      WRITE (6,80) PRCT(FE2), LOGX(FE2), GMX(FE2), PRCT(FE3),
      $LOGX(FE3), GMX(FE3)
80  FORMAT (10X, 'FE2 ', F8.3, F10.4, F7.3, 6X, 'FE3 ',
      $F8.3, F10.4, F7.3, //)
      WRITE (6,85) PRCT(FE2OH), LOGXY(FE2OH), GMXY(FE2OH), PRCT(FEOH),
      $LOGXY(FEOH), GMXY(FEOH)
85  FORMAT (10X, 'FE2OH ', F8.3, F10.4, F7.3, 6X, 'FEOH ',
      $F8.3, F10.4, F7.3, //)
      WRITE (6,90) PRCT(FE2OH2), LOGXY(FE2OH2), GMXY(FE2OH2),
      $PRCT(FEOH2), LOGXY(FEOH2), GMXY(FEOH2)
90  FORMAT (10X, 'FE2OH2 ', F8.3, F10.4, F7.3, 6X, 'FEOH2 ',
      $F8.3, F10.4, F7.3, //)
      WRITE (6,95) PRCT(FE2OH3), LOGXY(FE2OH3), GMXY(FE2OH3),
      $PRCT(FEOH3), LOGXY(FEOH3), GMXY(FEOH3)
95  FORMAT (10X, 'FE2OH3 ', F8.3, F10.4, F7.3, 6X, 'FEOH3 ',

```

```

    $F8.3, F10.4, F7.3, //)
    WRITE (6,100) PRCT(FE2SO4), LOGXY(FE2SO4), GMXY(FE2SO4),
    $PRCT(FEOH4), LOGXY(FEOH4), GMXY(FEOH4)
100 FORMAT (10X, 'FE2SO4 ', F8.3, F10.4, F7.3, 6X, 'FEOH4 ',
    $F8.3, F10.4, F7.3, //)
    WRITE (6,105) PRCT(FE2HSO), LOGXY(FE2HSO), GMXY(FE2HSO),
    $PRCT(FESO4), LOGXY(FESO4), GMXY(FESO4)
105 FORMAT (10X, 'FE2HSO ', F8.3, F10.4, F7.3, 6X, 'FESO4 ',
    $F8.3, F10.4, F7.3, //)
    WRITE (6,110) PRCT(FESO42), LOGXY(FESO42), GMXY(FESO42)
110 FORMAT (48X, 'FESO42 ', F8.3, F10.4, F7.3, //)
    WRITE (6,115) LOGX(H), GMX(H), PRCT(FEHSO4), LOGXY(FEHSO4),
    $GMXY(FEHSO4)
115 FORMAT (10X, 'H ', 8X, F10.4, F7.3, 6X, 'FEHSO4 ',
    $F8.3, F10.4, F7.3, //)
    WRITE (6,120) LOGY(OH), GMY(OH), PRCT(FeCl), LOGXY(FeCl),
    $GMXY(FeCl)
120 FORMAT (10X, 'OH ', 8X, F10.4, F7.3, 6X, 'FeCl ',
    $F8.3, F10.4, F7.3, //)
    WRITE (6,125) LOGY(SO4), GMY(SO4), PRCT(FeCl2), LOGXY(FeCl2),
    $GMXY(FeCl2)
125 FORMAT (10X, 'SO4 ', 8X, F10.4, F7.3, 6X, 'FeCl2 ',
    $F8.3, F10.4, F7.3, //)
    WRITE (6,130) LOGY(CL), GMY(CL), PRCT(FeCl3), LOGXY(FeCl3),
    $GMXY(FeCl3)
130 FORMAT (10X, 'CL ', 8X, F10.4, F7.3, 6X, 'FeCl3 ',
    $F8.3, F10.4, F7.3, //)
    WRITE (6, 135) LOGXY(HSO4), GMXY(HSO4), PRCT(DFeOH2),
    $LOGXY(DFeOH2), GMXY(DFeOH2)
135 FORMAT (10X, 'HSO4 ', 8X, F10.4, F7.3, 6X, 'DFeOH2 ',
    $F8.3, F10.4, F7.3, //)
    WRITE (6, 140) LOGXY(H2SO4), GMXY(H2SO4), PRCT(TFeOH4),
    $LOGXY(TFeOH4), GMXY(TFeOH4)
140 FORMAT (10X, 'H2SO4 ', 8X, F10.4, F7.3, 6X, 'TFeOH4 ',
    $F8.3, F10.4, F7.3, //)
    WRITE (6, 145) LOGXY(HCl), GMXY(HCl)
145 FORMAT (10X, 'HCL ', 8X, F10.4, F7.3, //)
    WRITE (6, 150) ITFE2, EH
150 FORMAT (10X, 'ITFE2 ', I6, 14X, 'EH', 4X, F10.8, //)
    WRITE (6, 155) ITFE3, RAT
155 FORMAT (10X, 'ITFE3 ', I6, 14X, 'RAT', 3X, F10.8)
C
C*****THIS IS THE EXIT STATEMENT FOR THE STEP UP PH DO LOOP.
    20 CONTINUE
    STOP
    END
C
C SUBROUTINE ISTR(IST, PH, MX, MY, MXY, GMX, GMY, GMXY)
C *****
C * SUBPROGRAM ISTR-CLW. CALCULATES HYDROGEN ION AND HYDROXYL *
C * CONC'NS FROM DEFINITION OF PH; ADJUSTS THE CHLORIDE CONC'N TO *
C * MAKE CHARGES BALANCE; AND CALCULATES THE IONIC STRENGTH OF THE *
C * SOLUTION ASSUMING COMPLETE DISSOCIATION. CONC'N DATA IS *
C * SUPPLIED BY THE MAIN PROGRAM INPUT. *

```



```

C *****
C
REAL MX, MY, MXY, PH, EH, CHGX, CHGY, IST, GMX, GMY, GMXY, CAPX,
$CAPY, CAPXY, AX, AY, AXY, TOTFE3, TOTFE2, SUMXY3, SUMXY2, SUMFE3,
$SUMFE2, LOGXY, LOGX, LOGY, R, PRCT
INTEGER H, FE2, FE3, OH, SO4, CL, X, Y, XY, ZX, ZY, ZXY, H2O,
$HSO4, H2SO4, HCL, FE2OH, FE2OH2, FE2OH3, FE2SO4, FE2HSO, FEOH,
$FEOH2, FEOH3, FEOH4, FESO4, FESO42, FEHSO4, FECL, FECL2, FECL3,
$DFEOH2, TFEOH4
DIMENSION ZX(3), ZY(3), ZXY(21), MX(3), MY(3), MXY(21), CAPX(3),
$CAPY(3), GMX(3), GMY(3), GMXY(21), AX(3), AY(3), AXY(21),
$LOGXY(21), LOGX(3), LOGY(3), PRCT(21)
DATA H, FE2, FE3/1, 2, 3/
DATA OH, SO4, CL/1, 2, 3/
DATA H2O, HSO4, H2SO4, HCL, FE2OH, FE2OH2, FE2OH3, FE2SO4,
$FE2HSO, FEOH, FEOH2, FEOH3, FEOH4, FESO4, FESO42, FEHSO4, FECL,
$FECL2, FECL3, DFEOH2, TFEOH4/1, 2, 3, 4, 5, 6, 7, 8, 9, 10, 11,
$12, 13, 14, 15, 16, 17, 18, 19, 20, 21/
DATA (ZX(I), I=1,3)/1, 2, 3/
DATA (ZY(J), J=1,3)/-1, -2, -1/
DATA (ZXY(L), L=1,21)/0, -1, 0, 0, 1, 0, -1, 0, 1, 2, 1, 0, -1,
$1, -1, 2, 2, 1, 0, 4, 5/
DATA (CAPX(X), X=1,3)/9.0, 6.0, 9.0/
DATA (CAPY(Y), Y=1,3)/3.5, 5.0, 3.5/
C
C*****CALCULATE HYDROGEN ION AND HYDROXYL CONCENTRATIONS FROM PH
C      ASSUMING ACTIVITY IS APPROX. EQUAL TO CONCENTRATION.
      MX(H)=10.0**(-PH)
      MY(OH)=10.0**(PH-14.0)
C
C*****CALCULATE TOTAL POSITIVE AND TOTAL NEGATIVE CHARGE
      CHGX=MX(FE2)*2.0+MX(FE3)*3.0+MX(H)
      CHGY=MY(CL)+MY(SO4)*2.0+MY(OH)
C*****ADJUST CHLORIDE CONCENTRATION TO MAKE CHARGES BALANCE
      MY(CL)=MY(CL)+(CHGX-CHGY)
C
C*****CALCULATE IONIC STRENGTH OF SOLUTION
      IST=0.0
      DO 20 X=1,3
        IST=IST+(0.5)*(MX(X))*(ZX(X)**2)
      20 CONTINUE
      DO 30 Y=1,3
        IST=IST+(0.5)*(MY(Y))*(ZY(Y)**2)
      30 CONTINUE
      RETURN
      END
C
C      SUBROUTINE GAMMA(IST, PH, MX, MY, MXY, GMX, GMY, GMXY)
C      *****
C      * SUBPROGRAM GAMMA-CLW. CALCULATES ACTIVITY COEFFICIENTS FOR *
C      * THE IONS AND ION PAIRS UNDER CONSIDERATION. THE VALUE OF THE *
C      * IONIC STRENGTH IS SUPPLIED BY THE SUBROUTINE ISTR-CLW. *
C      * THE EXTENDED DEBYE-HUCKEL EXPRESSION IS USED. *
C      *****

```

```

C
  REAL MX, MY, MXY, PH, EH, CHGX, CHGY, IST, GMX, GMY, GMXY, CAPX,
  $CAPY, CAPXY, AX, AY, AXY, TOTFE3, TOTFE2, SUMXY3, SUMXY2, SUMFE3,
  $SUMFE2
  INTEGER H, FE2, FE3, OH, SO4, CL, X, Y, XY, ZX, ZY, ZXY, H2O,
  $HSO4, H2SO4, HCL, FE2OH, FE2OH2, FE2OH3, FE2SO4, FE2HSO, FEOH,
  $FEOH2, FEOH3, FEOH4, FESO4, FESO42, FEHSO4, FECL, FECL2, FECL3,
  $DFEOH2, TFEOH4
  DIMENSION ZX(3), ZY(3), ZXY(21), MX(3), MY(3), MXY(21), CAPX(3),
  $CAPY(3), GMX(3), GMY(3), GMXY(21), AX(3), AY(3), AXY(21),
  $CAPXY(21)
  DATA H, FE2, FE3/1, 2, 3/
  DATA OH, SO4, CL/1, 2, 3/
  DATA H2O, HSO4, H2SO4, HCL, FE2OH, FE2OH2, FE2OH3, FE2SO4,
  $FE2HSO, FEOH, FEOH2, FEOH3, FEOH4, FESO4, FESO42, FEHSO4, FECL,
  $FECL2, FECL3, DFEOH2, TFEOH4/1, 2, 3, 4, 5, 6, 7, 8, 9, 10, 11,
  $12, 13, 14, 15, 16, 17, 18, 19, 20, 21/
  DATA (ZX(I), I=1,3)/1, 2, 3/
  DATA (ZY(J), J=1,3)/-1, -2, -1/
  DATA (ZXY(L), L=1,21)/0, -1, 0, 0, 1, 0, -1, 0, 1, 2, 1, 0, -1,
  $1, -1, 2, 2, 1, 0, 4, 5/
  DATA (CAPX(X), X=1,3)/9.0, 6.0, 9.0/
  DATA (CAPY(Y), Y=1,3)/3.5, 5.0, 3.5/
  DATA (CAPXY(XY), XY=1,21)/0.0, 4.5, 0.0, 0.0, 5.0, 0.0, 5.5, 0.0,
  $5.4, 5.0, 5.0, 0.0, 5.4, 5.0, 5.5, 6.0, 5.0, 5.0, 0.0, 11.0, 11.0/

C
C*****CONSTANT DEBYE-HUCKEL PARAMETERS
  AA=0.5098
  BB=0.3284

C
C*****CALCULATE ACTIVITY COEFFICIENTS
  DO 10 X=1,3
  DO 10 Y=1,3
  DO 10 XY=1,21
  GMX(X)=10.0**((-AA*(ZX(X)**2)*SQRT(IST))/(1.0+(CAPX(X)*BB*
  $SQRT(IST))))
  GMY(Y)=10.0**((-AA*(ZY(Y)**2)*SQRT(IST))/(1.0+(CAPY(Y)*BB*
  $SQRT(IST))))
  GMXY(XY)=10.0**((-AA*(ZXY(XY)**2)*SQRT(IST))/(1.0+(CAPXY(XY)*BB*
  $SQRT(IST))))
10 CONTINUE
  RETURN
  END

C
  SUBROUTINE DISTN(IST, PH, MX, MY, MXY, GMX, GMY, GMXY, TOTFE3,
  $TOTFE2, SUMFE2, SUMFE3, ITFE2, ITFE3, AX)
  C*****
  C * SUBPROGRAM DISTN-CLW. CALCULATES THE ACTIVITIES OF THE FREE *
  C * IONS USING ACTIVITY COEFFICIENTS SUPPLIED BY THE SUBROUTINE *
  C * GAMMA-CLW AND SINGLE ION CONCENTRATIONS SUPPLIED BY THE MAIN *
  C * PROGRAM INPUT. THE CONCENTRATION OF EACH ION PAIR IS THEN *
  C * CALCULATED USING ASSOCIATION PRODUCT EQUATIONS WITH ACTIVITY *
  C * COEFFICIENTS FOR THE ION PAIRS SUPPLIED BY THE SUBROUTINE *
  C * GAMMA-CLW. *

```

```

C      * A CONTINUOUS FRACTION ITERATION IS USED TO DETERMINE THE TRUE *
C      * VALUES FOR THE FREE UNASSOCIATED FERRIC AND FERROUS IONS. *
C      * THE ITERATION STOPS WHEN A DIFFERENCE OF LESS THAN 0.01 PERCENT*
C      * BETWEEN THE TOTAL MEASURED AND TOTAL CALCULATED VALUES IS *
C      * REACHED. *
C      *****
C
      REAL MX, MY, MXY, PH, EH, CHGX, CHGY, IST, GMX, GMY, GMXY, CAPX,
      $CAPY, CAPXY, AX, AY, AXY, TOTFE3, TOTFE2, SUMXY3, SUMXY2, SUMFE3,
      $SUMFE2
      INTEGER H, FE2, FE3, OH, SO4, CL, X, Y, XY, ZX, ZY, ZXY, H2O,
      $HSO4, H2SO4, HCL, FE2OH, FE2OH2, FE2OH3, FE2SO4, FE2HSO, FEOH,
      $FEOH2, FEOH3, FEOH4, FESO4, FESO42, FEHSO4, FECL, FECL2, FECL3,
      $DFEOH2, TFEOH4, ITFE2, ITFE3
      DIMENSION ZX(3), ZY(3), ZXY(21), MX(3), MY(3), MXY(21), CAPX(3),
      $CAPY(3), GMX(3), GMY(3), GMXY(21), AX(3), AY(3), AXY(21)
      DATA H, FE2, FE3/1, 2, 3/
      DATA OH, SO4, CL/1, 2, 3/
      DATA H2O, HSO4, H2SO4, HCL, FE2OH, FE2OH2, FE2OH3, FE2SO4,
      $FE2HSO, FEOH, FEOH2, FEOH3, FEOH4, FESO4, FESO42, FEHSO4, FECL,
      $FECL2, FECL3, DFEOH2, TFEOH4/1, 2, 3, 4, 5, 6, 7, 8, 9, 10, 11,
      $12, 13, 14, 15, 16, 17, 18, 19, 20, 21/
      DATA (ZX(I), I=1,3)/1, 2, 3/
      DATA (ZY(J), J=1,3)/-1, -2, -1/
      DATA (ZXY(L), L=1,21)/0, -1, 0, 0, 1, 0, -1, 0, 1, 2, 1, 0, -1,
      $1, -1, 2, 2, 1, 0, 4, 5/
      DATA (CAPX(X), X=1,3)/9.0, 6.0, 9.0/
      DATA (CAPY(Y), Y=1,3)/3.5, 5.0, 3.5/
C
C*****CALCULATE HYDROGEN AND HYDROXYL ACTIVITIES USING PH DEFINITION.
C      HYDROGEN AND HYDROXYL ACTIVITIES ARE NOW EQUAL TO CONC'N.
      AX(H)=10.0**(-PH)
      AY(OH)=10.0**(PH-14.0)
C
C*****CALCULATE CONC'N OF BISULFATE USING ITS ASSOCIATION CONSTANT
C      AND THE TOTAL SULFATE DISTRIBUTION EQUATION.
C      AT THIS POINT MY(SO4) REPRESENTS TOTAL SULFATE.
      MXY(HSO4)=((10.0**1.99)*(AX(H))*(GMY(SO4))*(MY(SO4)))/
      $( (GMXY(HSO4)) + ((10.0**1.99)*(AX(H))*(GMY(SO4))) )
C
C*****CALCULATE BISULFATE ACTIVITY. THIS VALUE WILL BE USED IN THE
C      ION PAIR CALCULATIONS.
      AXY(HSO4)=(GMXY(HSO4))*(MXY(HSO4))
C
C*****RECALCULATE CONC'N OF SULFATE ION. NOW MY(SO4) WILL REPRESENT
C      TRUE SULFATE ION CONC'N.
      MY(SO4)=MY(SO4)-MXY(HSO4)
C
C*****CALCULATE THE ACTIVITIES OF THE FREE IONS.
      DO 10 X=2,3
      AX(X)=GMX(X)*MX(X)
10  CONTINUE
      DO 20 Y=2,3
      AY(Y)=GMY(Y)*MY(Y)

```

```

20 CONTINUE
C
C*****THE ORIGINAL MX(FE3) AND MX(FE2) VALUES ARE EQUAL TO THE
C      TOTAL CONC'NS FOR FERRIC AND FERROUS, RESPECTIVELY.
C      CONTINUOUS FRACTION ITERATION BEGINS BY GUESSING THAT MX(FE3)
C      REPRESENTS THE FREE FERRIC ION CONC'N.  USE THE AX(FE3)
C      CALCULATED ABOVE FROM MX(FE3) AND GMX(FE3) TO DETERMINE
C      CONC'NS OF ION PAIRS.
C*****ITFE3 IS THE ITERATION COUNTER FOR FERRIC
      ITFE3=1
C
30 MXY(HSO4)=((10.0**1.99)*(AX(1))*(AY(2)))/(GMXY(2))
C
      MXY(H2SO4)=((10.0**(-3.0))*(AX(1))*(AXY(2)))/(GMXY(3))
C
      MXY(HCL)=((10.0**(-3.0))*(AX(1))*(AY(3)))/(GMXY(4))
C
C
      MXY(FEOH)=((10.0**11.91)*(AX(3))*(AY(1)))/(GMXY(10))
C
      MXY(FEOH2)=((10.0**22.33)*(AX(3))*((AY(1))**2))/(GMXY(11))
C
      MXY(FEOH3)=((10.0**30.0)*(AX(3))*((AY(1))**3))/(GMXY(12))
C
      MXY(FEOH4)=((10.0**34.4)*(AX(3))*((AY(1))**4))/(GMXY(13))
C
      MXY(FESO4)=((10.0**4.04)*(AX(3))*(AY(2)))/(GMXY(14))
C
      MXY(FESO42)=((10.0**5.40)*(AX(3))*((AY(2))**2))/(GMXY(15))
C
      MXY(FEH2SO4)=((10.0**0.6)*(AX(3))*(AXY(2)))/(GMXY(16))
C
      MXY(FECL)=((10.0**1.48)*(AX(3))*(AY(3)))/(GMXY(17))
C
      MXY(FECL2)=((10.0**2.13)*(AX(3))*((AY(3))**2))/(GMXY(18))
C
      MXY(FECL3)=((10.0**(-0.7))*(AX(3))*((AY(3))**3))/(GMXY(19))
C
      MXY(DFEOH2)=((10.0**25.05))*((AX(3))**2)*((AY(1))**2))/(GMXY(20))
C
      MXY(TFEOH4)=((10.0**49.7))*((AX(3))**3)*((AY(1))**4))/(GMXY(21))
C
C*****CALCULATE THE SUM OF THE CONC'NS OF FERRIC ION PAIR SPECIES.
      SUMXY3=0.0
      DO 40 I=10,21
        SUMXY3=SUMXY3+MXY(I)
40 CONTINUE
C
C*****CALCULATE THE SUM OF ALL FERRIC SPECIES.
      SUMFE3=SUMXY3+MX(FE3)
C
C*****TEST THE DIFFERENCE BETWEEN TOTAL FERRIC IRON CONC'N AND THE
C      SUM OF CONC'NS OF ALL FERRIC IRON SPECIES JUST DETERMINED.
      IF((ABS((TOTFE3/SUMFE3)-1.0)) .LE. 0.0001) GO TO 50

```

```

C
C*****IF THE DIFFERENCE IS NOT LESS THAN 0.01 PERCENT, ADJUST THE
C      MX(FE3) GUESS BY MULTIPLYING BY THE RATIO OF TRUE TOTAL FERRIC
C      TO CALCULATED TOTAL FERRIC.
C      MX(FE3)=MX(FE3)*(TOTFE3/SUMFE3)
C
C*****RECALCULATE THE ACTIVITY OF FREE FERRIC ION AND RETURN TO THE
C      ION PAIR CONC'N EQUATIONS FOR A NEW ITERATION.
C      AX(FE3)=GMX(FE3)*MX(FE3)
C
C*****ITFE3 IS THE ITERATION COUNTER FOR FERRIC
C      ITFE3=ITFE3+1
C
C      GO TO 30
C
C*****THE FOLLOWING IS A SIMILAR ITERATION FOR FERROUS IRON.
C*****ITFE2 IS THE ITERATION COUNTER FOR FERROUS
C      50 ITFE2=1
C
C      55 MXY(FE2OH)=((10.0**4.5)*(AX(2))*(AY(1)))/(GMXY(5))
C
C      MXY(FE2OH2)=((10.0**7.4)*(AX(2))*((AY(1))**2))/(GMXY(6))
C
C      MXY(FE2OH3)=((10.0**11.0)*(AX(2))*((AY(1))**3))/(GMXY(7))
C
C      MXY(FE2SO4)=((10.0**2.2)*(AX(2))*(AY(2)))/(GMXY(8))
C
C      MXY(FE2HSO)=((10.0**1.1)*(AX(2))*(AXY(2)))/(GMXY(9))
C
C      SUMXY2=0.0
C      DO 60 I=5,9
C      SUMXY2=SUMXY2+MXY(I)
C      60 CONTINUE
C
C      SUMFE2=SUMXY2+MX(FE2)
C      IF((ABS((TOTFE2/SUMFE2)-1.0)) .LE. 0.0001) GO TO 100
C      MX(FE2)=MX(FE2)*(TOTFE2/SUMFE2)
C      AX(FE2)=GMX(FE2)*MX(FE2)
C      ITFE2=ITFE2+1
C
C      GO TO 55
C      100 CONTINUE
C      RETURN
C      END
C$ENTRY
C      0.01      0.00100001 0.00100000

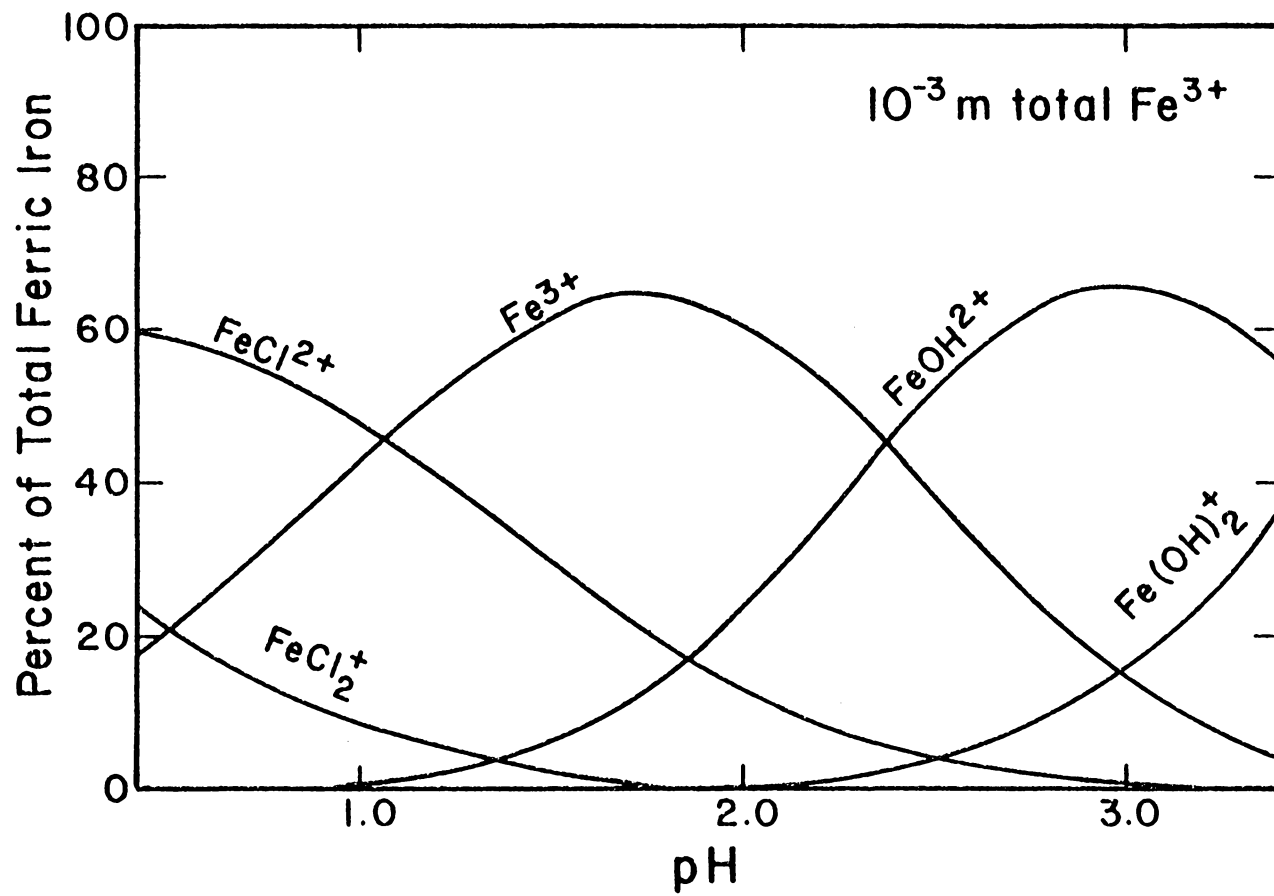
```

Figure 4: Example output produced by the program IRON.

PH=2.00 IST= 0.0160 TITFE2=0.000000 TITFE3=0.001000 MSD4=0.000000
 TUIFE=0.001000 SUMFE2=0.000000 SUMFE3=0.001000 MCL= 0.010000

SPECIES FERROUS	PRCT	LOGC	GAMMA	SPECIES FERRIC	PRCT	LOGC	GAMMA
FE2	100.000	-7.9995	0.622	FE3	61.198	-3.2133	0.378
FE2OH	0.000	-15.6526	0.884	FEUH	24.428	-3.6121	0.612
FE2OH2	0.000	-24.8060	1.000	FEUH2	0.559	-5.2523	0.884
FE2OH3	0.000	-33.1535	0.886	FEUH3	0.000	-9.6357	1.000
FE2SO4	0.000	-15.2887	1.000	FEUH4	0.000	-17.1830	0.886
FE2HSD	0.000	-16.3461	0.886	FESO4	0.000	-8.8251	0.884
				FESO42	0.000	-16.7487	0.886
H		-2.0000	0.898	FEHSO4	0.000	-12.1220	0.622
OH		-12.0000	0.878	FECL	13.047	-3.8845	0.612
SO4		-9.0692	0.612	FECL2	0.460	-5.3370	0.884
CL		-1.8861	0.878	FECL3	0.000	-10.1628	1.000
HSO4		-9.2384	0.882	DFEOH2	0.307	-5.5132	0.196
H2SO4		-14.2928	1.000	TFEOH4	0.001	-8.1006	0.078
HCL		-6.9424	1.000				
ITFE2	1		EH	1.02873100			
ITFE3	3		RAT	*****			

Figure 5: Speciation diagram constructed from pH versus percent of total ferric iron data calculated by the program IRON.



REDOX - A PROGRAM TO CALCULATE IRON REDOX EQUILIBRIA IN ACID CHLORIDE SOLUTIONS

REDOX is a FORTRAN program which calculates iron redox equilibria at 25°C using a modification of the program IRON described above. It was designed to calculate the total stoichiometric activity coefficient ratio, $\gamma(R)$, for the ferric-ferrous activity ratio at a specific pH, and, using this value, to calculate the concentrations of free ferric and free ferrous iron corresponding to a given Eh and total iron concentration. REDOX consists of a main program IRONB, which is a modified version of IRON's main program IRONA, the subroutines ISTR, GAMMA, and DISTN as described above, and an additional subroutine REDOXS. REDOXS is described separately below.

Input data is obtained from measurements made on run solutions in FeS₂ oxidation experiments. Input format is 5F10.0 and consists of MCL, TOTFE, and TOTFE3 as in IRON, along with measured pH and EMF (in volts). The remainder of the main program IRONB is identical to IRONA except that the pH value is set by the input, an additional subroutine, REDOXS, is called after the speciation calculations instead of calculating Eh from the activity ratio, and the output lists values for the additional variables TAC, M3EH, and M2EH.

REDOXS: Using input data and values calculated by the preceding subroutines, REDOXS performs the following functions:

- 1) Calculation of the total stoichiometric activity coefficient ratio, $\gamma(R)$, for ferric-ferrous. The total stoichiometric activity coefficient for a particular species *i* in solution is given by

$$\gamma(\text{TOT})_i = \gamma_i \gamma(\text{CPLX})_i$$

where γ_i is the molal Debye-Huckel individual ionic activity coefficient which accounts for short-range, ion-pairing effects, and $\gamma(\text{CPLX})_i$ is a coefficient which corrects for the percentage of the total amount of that species, i , in solution that remains uncomplexed. $\gamma(\text{CPLX})_i$ is found by dividing the concentration of the free uncomplexed ionic species, i , by the total concentration of i in solution. The value for $\gamma(\text{R})$, then, is given by

$$\gamma(\text{R}) = (\gamma(\text{TOT})_{\text{Fe}^{3+}} / \gamma(\text{TOT})_{\text{Fe}^{2+}}).$$

- 2) Calculation of the concentration of free ferric iron corresponding to the EMF (Eh) and TOTFE input values. Equation 16 as derived in the text of this paper is used here:

$$m_{\text{Fe}^{3+}} = m_{\text{Fe}^{3+}}^0 [\exp X / (\gamma(\text{R}) + \exp X)]$$

without the 7% correction for increase in total iron. M3EH is the symbol used for the concentration of free ferric iron as calculated from the Eh, and M2EH is the free ferrous concentration calculated by difference, TOTFE - M3EH.

Listings of the main program IRONB and the subroutine REDOXS are included below. An example of input format can be found at the end of the REDOXS listing. An example of the output is shown in Figure 6.

IRONB LISTINGMAIN PROGRAM OF REDOX

```

C$JOB          RIMSTIDT
C$OPTIONS NOLIST
C *****
C * PROGRAM IRONB::8-30-82::C.L. WIERSMA *
C * A PROGRAM TO CALCULATE IRON REDOX EQUILIBRIA AT 25 DEGREES *
C * CELSIUS. INPUT DATA ARE MOLAL CONCENTRATIONS OF MAJOR IONS, *
C * PH, AND EMF IN VOLTS. *
C *****
C
C      REAL MX, MY, MXY, PH, EH, CHGX, CHGY, IST, GMX, GMY, GMXY, CAPX,
$CAPY, CAPXY, AX, AY, AXY, TOTFE3, TOTFE2, SUMXY3, SUMXY2, SUMFE3,
$SUMFE2, LOGXY, LOGX, LOGY, R, PRCT, MSO4, MCL,
STAC, C, M3EH, M2EH, RAT, TOTFE, EMF
C      INTEGER H, FE2, FE3, OH, SO4, CL, X, Y, XY, ZX, ZY, ZXY, H2O,
$HSO4, H2SO4, HCL, FE2OH, FE2OH2, FE2OH3, FE2SO4, FE2HSO, FEOH,
$FEOH2, FEOH3, FEOH4, FESO4, FESO42, FEHSO4, FECL, FECL2, FECL3,
$DFEOH2, TFEOH4, ITFE2, ITFE3
C      DIMENSION ZX(3), ZY(3), ZXY(21), MX(3), MY(3), MXY(21), CAPX(3),
$CAPY(3), GMX(3), GMY(3), GMXY(21), AX(3), AY(3), AXY(21),
$LOGXY(21), LOGX(3), LOGY(3), PRCT(21)
C      DATA H, FE2, FE3/1, 2, 3/
C      DATA OH, SO4, CL/1, 2, 3/
C      DATA H2O, HSO4, H2SO4, HCL, FE2OH, FE2OH2, FE2OH3, FE2SO4,
$FE2HSO, FEOH, FEOH2, FEOH3, FEOH4, FESO4, FESO42, FEHSO4, FECL,
$FECL2, FECL3, DFEOH2, TFEOH4/1, 2, 3, 4, 5, 6, 7, 8, 9, 10, 11,
$12, 13, 14, 15, 16, 17, 18, 19, 20, 21/
C      DATA (ZX(I), I=1,3)/1, 2, 3/
C      DATA (ZY(J), J=1,3)/-1, -2, -1/
C      DATA (ZXY(L), L=1,21)/0, -1, 0, 0, 1, 0, -1, 0, 1, 2, 1, 0, -1,
$1, -1, 2, 2, 1, 0, 4, 5/
C      DATA (CAPX(X), X=1,3)/9.0, 6.0, 9.0/
C      DATA (CAPY(Y), Y=1,3)/3.5, 5.0, 3.5/
C
C *****INPUT-READ CONC'NS OF IONS, PH AND EMF
C      READ (5,10) MCL, TOTFE, TOTFE3, PH, EMF
C      10 FORMAT (5F10.0)
C
C      TOTFE2=TOTFE-TOTFE3
C      MSO4=(TOTFE2)/7.0
C      MX(FE2)=TOTFE2
C      MX(FE3)=TOTFE3
C      MY(SO4)=MSO4
C      MY(CL)=MCL
C      15 CALL ISTR(IST, PH, MX, MY, MXY, GMX, GMY, GMXY)
C      CALL GAMMA(IST, PH, MX, MY, MXY, GMX, GMY, GMXY)
C      CALL DISTN(IST, PH, MX, MY, MXY, GMX, GMY, GMXY, TOTFE3, TOTFE2,
$SUMFE2, SUMFE3, ITFE2, ITFE3, TOTFE)
C
C *****CALCULATE WHAT PERCENT OF THE TOTAL IRON EACH SPECIES

```

```

C      REPRESENTS.
      PRCT(FE3)=(MX(FE3)/TOTFE3)*100.0
      DO 25 M=10,21
25     PRCT(M)=(MXY(M)/TOTFE3)*100.0
      PRCT(FE2)=(MX(FE2)/TOTFE2)*100.0
      DO 26 N=5,9
26     PRCT(N)=(MXY(N)/TOTFE2)*100.0
C
      CALL REDOXS(EH, GMX, TOTFE3, PRCT, TAC, C, M3EH, M2EH, RAT,
      $TOTFE, EMF)
C
C*****TAKE THE LOG OF THE CONCENTRATION VALUES TO FACILITATE DATA
C      PLOTTING WHEN THE ITERATION IS COMPLETED.
      DO 30 J=2,21
      LOGXY(J)=ALOG10(MXY(J))
30     CONTINUE
      DO 40 K=1,3
      LOGX(K)=ALOG10(MX(K))
40     CONTINUE
      DO 50 L=1,3
      LOGY(L)=ALOG10(MY(L))
50     CONTINUE
C
C*****PRINT OUTPUT WHEN ITERATION IS COMPLETED.
      WRITE (6,60) PH, IST, TOTFE2, TOTFE3, MSO4
60     FORMAT (1H1, 10X, 'PH=', F4.2, 6X, 'IST=', F7.4, 6X, 'TOTFE2=',
      $F8.6, 6X, 'TOTFE3=', F8.6, 6X, 'MSO4=', F10.7)
      WRITE (6,65) TOTFE, SUMFE2, SUMFE3, MCL
65     FORMAT (22X, 'TOTFE=', F8.6, 5X,
      $'SUMFE2=', F8.6, 6X, 'SUMFE3=', F8.6, 6X, 'MCL =',
      $F10.7, ///)
      WRITE (6,70)
70     FORMAT (10X, 'SPECIES', 4X, 'PRCT', 4X, 'LOGC', 4X, 'GAMMA', 6X,
      $'SPECIES', 4X, 'PRCT', 4X, 'LOGC', 4X, 'GAMMA')
      WRITE (6,75)
75     FORMAT (10X, 'FERROUS', 31X, 'FERRIC', //)
      WRITE (6,80) PRCT(FE2), LOGX(FE2), GMX(FE2), PRCT(FE3),
      $LOGX(FE3), GMX(FE3)
80     FORMAT (10X, 'FE2 ', F8.3, F10.4, F7.3, 6X, 'FE3 ',
      $F8.3, F10.4, F7.3, //)
      WRITE (6,85) PRCT(FE2OH), LOGXY(FE2OH), GMXY(FE2OH), PRCT(FEOH),
      $LOGXY(FEOH), GMXY(FEOH)
85     FORMAT (10X, 'FE2OH ', F8.3, F10.4, F7.3, 6X, 'FEOH ',
      $F8.3, F10.4, F7.3, //)
      WRITE (6,90) PRCT(FE2OH2), LOGXY(FE2OH2), GMXY(FE2OH2),
      $PRCT(FEOH2), LOGXY(FEOH2), GMXY(FEOH2)
90     FORMAT (10X, 'FE2OH2 ', F8.3, F10.4, F7.3, 6X, 'FEOH2 ',
      $F8.3, F10.4, F7.3, //)
      WRITE (6,95) PRCT(FE2OH3), LOGXY(FE2OH3), GMXY(FE2OH3),
      $PRCT(FEOH3), LOGXY(FEOH3), GMXY(FEOH3)
95     FORMAT (10X, 'FE2OH3 ', F8.3, F10.4, F7.3, 6X, 'FEOH3 ',
      $F8.3, F10.4, F7.3, //)
      WRITE (6,100) PRCT(FE2SO4), LOGXY(FE2SO4), GMXY(FE2SO4),
      $PRCT(FEOH4), LOGXY(FEOH4), GMXY(FEOH4)

```

```

100 FORMAT (10X, 'FE2SO4 ', F8.3, F10.4, F7.3, 6X, 'FEOH4 ',
    $F8.3, F10.4, F7.3, //)
    WRITE (6,105) PRCT(FE2HSO), LOGXY(FE2HSO), GMXY(FE2HSO),
    $PRCT(FESO4), LOGXY(FESO4), GMXY(FESO4)
105 FORMAT (10X, 'FE2HSO ', F8.3, F10.4, F7.3, 6X, 'FESO4 ',
    $F8.3, F10.4, F7.3, //)
    WRITE (6,110) PRCT(FESO42), LOGXY(FESO42), GMXY(FESO42)
110 FORMAT (48X, 'FESO42 ', F8.3, F10.4, F7.3, //)
    WRITE (6,115) LOGX(H), GMX(H), PRCT(FEHSO4), LOGXY(FEHSO4),
    $GMXY(FEHSO4)
115 FORMAT (10X, 'H ', 8X, F10.4, F7.3, 6X, 'FEHSO4 ',
    $F8.3, F10.4, F7.3, //)
    WRITE (6,120) LOGY(OH), GMY(OH), PRCT(FECL), LOGXY(FECL),
    $GMXY(FECL)
120 FORMAT (10X, 'OH ', 8X, F10.4, F7.3, 6X, 'FECL ',
    $F8.3, F10.4, F7.3, //)
    WRITE (6,125) LOGY(SO4), GMY(SO4), PRCT(FECL2), LOGXY(FECL2),
    $GMXY(FECL2)
125 FORMAT (10X, 'SO4 ', 8X, F10.4, F7.3, 6X, 'FECL2 ',
    $F8.3, F10.4, F7.3, //)
    WRITE (6,130) LOGY(CL), GMY(CL), PRCT(FECL3), LOGXY(FECL3),
    $GMXY(FECL3)
130 FORMAT (10X, 'CL ', 8X, F10.4, F7.3, 6X, 'FECL3 ',
    $F8.3, F10.4, F7.3, //)
    WRITE (6,135) LOGXY(HSO4), GMXY(HSO4), PRCT(DFEOH2),
    $LOGXY(DFEOH2), GMXY(DFEOH2)
135 FORMAT (10X, 'HSO4 ', 8X, F10.4, F7.3, 6X, 'DFEOH2 ',
    $F8.3, F10.4, F7.3, //)
    WRITE (6,140) LOGXY(H2SO4), GMXY(H2SO4), PRCT(TFEOH4),
    $LOGXY(TFEOH4), GMXY(TFEOH4)
140 FORMAT (10X, 'H2SO4 ', 8X, F10.4, F7.3, 6X, 'TFEOH4 ',
    $F8.3, F10.4, F7.3, //)
    WRITE (6,145) LOGXY(HCL), GMXY(HCL), TAC
145 FORMAT (10X, 'HCL ', 8X, F10.4, F7.3, 6X, 'TAC ',
    $F10.7, //)
    WRITE (6,150) ITFE2, EH, M3EH
150 FORMAT (10X, 'ITFE2 ', I6, 14X, 'EH', 4X, F10.8, 5X,
    $'M3EH', 4X, F10.8, //)
    WRITE (6,155) ITFE3, RAT, M2EH
155 FORMAT (10X, 'ITFE3 ', I6, 14X, 'RAT', 3X, F10.8, 5X,
    $'M2EH', 4X, F10.8)

```

C

```

STOP
END

```

C

REDOXS SUBROUTINE LISTING

SUBROUTINE OF REDOX

```

SUBROUTINE REDOXS(EH, GMX, TOTFE3, PRCT, TAC, C, M3EH, M2EH, RAT,
$TOTFE, EMF)
C *****
C * SUBROUTINE REDOXS-CLW. REDOX EQUILIBRIA CALCULATIONS AT 25 *
C * DEGREES CELSIUS. CALCULATES THE TOTAL FERRIC IRON CONCENT- *
C * TRATION CORRESPONDING TO A GIVEN EMF MEASUREMENT AND GIVEN *
C * INITIAL TOTAL IRON CONCENTRATION, USING THE NERNST EQUATION *
C * AND ACTIVITY RELATIONS. *
C *****
C
REAL MX, MY, MXY, PH, EH, CHGX, CHGY, IST, GMX, GMY, GMXY, CAPX,
$CAPY, CAPXY, AX, AY, AXY, TOTFE3, TOTFE2, SUMXY3, SUMXY2, SUMFE3,
$SUMFE2, LOGXY, LOGX, LOGY, R, PRCT, M$O4, MCL,
$TAC, C, M3EH, M2EH, RAT, TOTFE, EMF
INTEGER H, FE2, FE3, OH, SO4, CL, X, Y, XY, ZX, ZY, ZXY, H2O,
$HSO4, H2SO4, HCL, FE2OH, FE2OH2, FE2OH3, FE2SO4, FE2HSO, FEOH,
$FEOH2, FEOH3, FEOH4, FESO4, FESO42, FEHSO4, FECL, FECL2, FECL3,
$DFEOH2, TFEOH4, ITFE2, ITFE3
DIMENSION ZX(3), ZY(3), ZXY(21), MX(3), MY(3), MXY(21), CAPX(3),
$CAPY(3), GMX(3), GMY(3), GMXY(21), AX(3), AY(3), AXY(21),
$LOGXY(21), LOGX(3), LOGY(3), PRCT(21)
DATA H, FE2, FE3/1, 2, 3/
DATA OH, SO4, CL/1, 2, 3/
DATA H2O, HSO4, H2SO4, HCL, FE2OH, FE2OH2, FE2OH3, FE2SO4,
$FE2HSC, FEOH, FEOH2, FEOH3, FEOH4, FESO4, FESO42, FEHSO4, FECL,
$FECL2, FECL3, DFEOH2, TFEOH4/1, 2, 3, 4, 5, 6, 7, 8, 9, 10, 11,
$12, 13, 14, 15, 16, 17, 18, 19, 20, 21/
DATA (ZX(I), I=1,3)/1, 2, 3/
DATA (ZY(J), J=1,3)/-1, -2, -1/
DATA (ZXY(L), L=1,21)/0, -1, 0, 0, 1, 0, -1, 0, 1, 2, 1, 0, -1,
$1, -1, 2, 2, 1, 0, 4, 5/
DATA (CAPX(X), X=1,3)/9.0, 6.0, 9.0/
DATA (CAPY(Y), Y=1,3)/3.5, 5.0, 3.5/
C
C*****CALCULATE THE TOTAL ACTIVITY COEFFICIENT
TAC=(GMX(FE3)/GMX(FE2))*(PRCT(FE3)/PRCT(FE2))
C
C*****CALCULATE EH FROM EMF + REFERENCE CELL POTENTIAL
EH=EMF+0.19483
C
C*****CALCULATE THE CONSTANT IN THE EXPONENTIAL
C=(EH-0.771)/(0.02569)
C
C*****CALCULATE THE TOTAL CONCENTRATION OF FERRIC IRON CORRESPONDING
C TO THE INPUT MEASURED EMF VALUE. HERE TOTFE3 IS INITIAL TOTAL
C FERRIC = INITIAL TOTAL IRON.
M3EH=(TOTFE)*(EXP(C)/(TAC+EXP(C)))
C
C*****CALCULATE THE TOTAL FERROUS CONCENTRATION

```

```
      M2EH=TOTFE-M3EH
C
C*****CALCULATE THE ACTIVITY RATIO OF FERRIC TO FERROUS USING THE
C      NERNST RELATION.
      RAT=EXP(C)
      RETURN
      END
C
C$ENTRY
      0.01  0.0010701  0.0010700  2.01  0.72301
```


Figure 6: Example output produced by the program REDOX.

PH=2.00

ISI= 0.0162
TOTFE=0.001030

TOTFE2=0.000000
SUMFE2=0.000000

TOTFE3=0.001030
SUMFE3=0.001030

MSO4= 0.000000
MCL = 0.010000

SPECIES FERROUS	PRCT	LOGC	GAMMA	SPECIES FERRIC	PRCT	LOGC	GAMMA
FE2	100.000	-9.0309	0.620	FE3	61.180	-3.2008	0.377
FE2OH	0.000	-16.6846	0.884	FEUH	24.380	-3.6003	0.610
FE2OH2	0.000	-25.8383	1.000	FEUH2	0.557	-5.2413	0.884
FE2OH3	0.000	-34.1856	0.886	FEUH3	0.000	-9.6249	1.000
FE2SO4	0.000	-17.3531	1.000	FEUH4	0.000	-17.1720	0.885
FE2HSO	0.000	-18.4102	0.885	FESO4	0.000	-9.8461	0.884
				FESO42	0.000	-18.8019	0.886
H		-2.0000	0.897	FEHSO4	0.000	-13.1424	0.620
OH		-12.0000	0.878	FECL	13.103	-3.8700	0.610
SO4		-10.1003	0.610	FECL2	0.464	-5.3206	0.884
CL		-1.8831	0.878	FECL3	0.000	-10.1439	1.000
HSO4		-10.2703	0.882	DFEOH2	0.315	-5.4889	0.195
H2SO4		-15.3249	1.000	TFEOH4	0.001	-8.0640	0.077
HCL		-6.9397	1.000	TAC	0.3714253		
ITFE2	1		EH	0.92223600	M3EH	0.00102844	
ITFE3	3		RAT	*****	M2EH	0.00000106	

**The vita has been removed from
the scanned document**

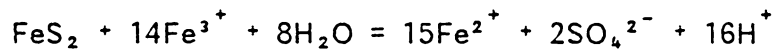
RELATIVE RATES OF REACTION OF
PYRITE AND MARCASITE
WITH FERRIC IRON AT LOW pH

by

Cynthia Leigh Wiersma

(ABSTRACT)

The relative reactivities of pulverized samples (100-200 mesh) of 3 marcasite and 7 pyrite specimens from various sources were determined at 25°C and pH = 2.0 in ferric chloride solutions with initial ferric iron concentrations of 10^{-3} molal. The rate of the reaction:



was determined by calculating the rate of reduction of aqueous ferric ion from measured oxidation-reduction potentials. The reaction follows the rate law:

$$-d m_{\text{Fe}^{3+}} / dt = k (A/M) m_{\text{Fe}^{3+}}$$

where $m_{\text{Fe}^{3+}}$ is the molal concentration of uncomplexed ferric iron, k is the rate constant and A/M is the surface area of reacting solid to mass of solution ratio. The measured rate constants, k , range from 1.0×10^{-4} to $2.7 \times 10^{-4} \text{ sec}^{-1} \pm 5\%$, with lower-temperature/early diagenetic pyrite having the smallest rate constants, marcasite intermediate, and pyrite of higher-temperature hydrothermal and metamorphic origin

having the greatest rate constants. Geologically, these small relative differences between the rate constants are not significant, so the fundamental reactivities of marcasite and pyrite are not appreciably different.

The activation energy of the reaction for a hydrothermal pyrite in the temperature interval of 25 to 50°C is 92 kJ mol⁻¹. The BET-measured specific surface area for lower-temperature/early diagenetic pyrite is an order of magnitude greater than that for pyrite of higher-temperature origin. Consequently, since the lower-temperature types have a much greater A/M ratio, they will appear to be more reactive per unit mass than the higher temperature types.